The effect of residual Ca^{2+} on the stochastic gating of Ca^{2+}-regulated Ca^{2+} channel models

Borbala Mazzag, Christopher J. Tignanelli and Gregory D. Smith

Department of Applied Science
College of William and Mary
Williamsburg, VA 23187

[Submitted July 1, 2004 to *Journal of Theoretical Biology*]

[Revised and resubmitted December 23, 2004.]

[Accepted December 27, 2004.]

Correspondence to: Gregory D. Smith
Department of Applied Science
McGlothlin-Street Hall, Rm 305
College of William and Mary
Williamsburg, VA 23187

greg@as.wm.edu

http://www.as.wm.edu/Faculty/Smith.html

Keywords: residual calcium, stochastic gating, intracellular calcium channel.

Abstract

Single channel models of intracellular Ca^{2+} channels such as the inositol 1,4,5-trisphosphate receptor and ryanodine receptor often assume that Ca^{2+}-dependent transitions are mediated by a constant background $[Ca^{2+}]$ as opposed to a dynamic $[Ca^{2+}]$ representing the formation and collapse of a localized Ca^{2+} domain. This assumption neglects the fact that Ca^{2+} released by open intracellular Ca^{2+} channels may influence subsequent gating through the processes of Ca^{2+}-activation or Ca^{2+}-inactivation. We study the effect of such "residual Ca^{2+}" from previous channel opening on the stochastic gating of minimal and realistic single channel models coupled to a restricted cytoplasmic compartment. Using Monte-Carlo simulation as well as analytical and numerical solution of a system of advection-reaction equations for the probability density of the domain $[Ca^{2+}]$ conditioned on the state of the channel, we determine how the steady-state open probability (p_{open}) of single channel models of Ca^{2+}-regulated Ca^{2+} channels depends on the time constant for Ca^{2+} domain formation and collapse. As expected, p_{open} for a minimal model including Ca^{2+} activation increases as the domain time constant becomes large compared to the open and closed dwell times of the channel, that is, on average the channel is activated by residual Ca^{2+} from previous openings. Interestingly, p_{open} for a channel model that is inactivated by Ca^{2+} also increases as a function of the domain time constant when the maximum domain $[Ca^{2+}]$ is fixed, because slow formation of the Ca^{2+} domain attenuates Ca^{2+}-mediated inactivation. Conversely, when the source amplitude of the channel is fixed, increasing the domain time constant leads to elevated domain $[Ca^{2+}]$ and decreased open probability. Consistent with these observations, a realistic De Young-Keizer-like IP_3R model responds to residual Ca^{2+} with a steady state open probability that is a monotonic function of the domain time constant, though minimal models that include both Ca^{2+}-activation and Ca^{2+}-inactivation show more complex behavior. We show how the probability density approach described here can be generalized for arbitrarily complex channel models and for any value of the domain time constant. In addition, we present a comparatively simple numerical procedure for estimating p_{open} for models of Ca^{2+}-regulated Ca^{2+} channels in the limit of a very fast or very slow Ca^{2+} domain. When the ordinary differential equation for the $[Ca^{2+}]$ in a restricted cytoplasmic compartment is replaced by a partial differential equation for the buffered diffusion of intracellular Ca^{2+} in a homogeneous isotropic cytosol, we find the dependence of p_{open} on the buffer time constant is qualitatively similar to the above mentioned results.

1 Introduction

Many ionic channels of excitable and non-excitable cells are regulated by the binding of intracellular Ca^{2+} and this regulation is often spatially localized. For example, in sensory hair cells of the inner ear Ca^{2+}-regulated potassium channels are activated by increases in the local [Ca^{2+}] due to the Ca^{2+} influx via spatially localized voltage-gated Ca^{2+} channels (Roberts, 1993; Roberts, 1994). In the process of excitation-contraction coupling in cardiac myocytes, Ca^{2+} influx via L-type Ca^{2+} channels (dihydropyridine receptors) into a restricted cytoplasmic compartment leads to activation of clusters of ryanodine receptors, sarcoplasmic reticulum Ca^{2+} release, and muscle cell contraction (Bers, 1992; Cheng *et al.*, 1993; Cannell *et al.*, 1995). Conversely, Ca^{2+} domains associated with voltage-gated and store-operated Ca^{2+} channels of the plasma membrane often promote inactivation (Sherman *et al.*, 1990; Zweifach & Lewis, 1995; Fierro & Parekh, 1999; Parekh, 2003). In this case, the stochastic gating of plasma membrane Ca^{2+} channels is influenced by the elevated [Ca^{2+}] due to Ca^{2+} release in a manner dependent on the unitary current of the channel and the composition and concentration of cytosolic Ca^{2+} buffers, including both endogenous Ca^{2+} binding proteins and exogenous Ca^{2+} chelators such as EGTA and BAPTA.

Intracellular Ca^{2+} channels such as inositol 1,4,5-trisphosphate receptors (IP_3Rs) and ryanodine receptors (RyRs) are also influenced by localized increases in [Ca^{2+}] that are a consequence of channel opening. For example, type 1 IP_3Rs reconstituted into planar lipid bilayers exhibit a decrease in open probability as the Ca^{2+} to Sr^{2+} molar ratio is increased in the *trans* chamber corresponding to the endoplasmic reticulum (ER) lumen (Bezprozvanny & Ehrlich, 1994). Bezprozvanny and Ehrlich hypothesized that this decrease in open probability is due to an increase in inhibitory Ca^{2+}-feedback onto the open IP_3R. Conversely, because domain [Ca^{2+}] near open intracellular Ca^{2+} channels depends on the driving force for Ca^{2+}, decreasing the [Ca^{2+}] difference between ER and cytosol will decrease the cytosolic Ca^{2+} domain amplitude and thereby attenuate domain Ca^{2+}-mediated inactivation of IP_3Rs. Enhanced IP_3R inactivation mediated by elevated ER Ca^{2+} has similarly been hypothesized to account for the persistence of Ca^{2+} oscillations in pituitary gonadotrophs as the ER concentration decreases during agonist-stimulated Ca^{2+} oscillations in Ca^{2+} free extracellular media (Li & Rinzel, 1994; Li *et al.*, 1995; Smith, 2002*b*). The feedback of Ca^{2+} domains on channel gating and/or direct lumenal regulation may be part of the explanation for differences in steady-state open probability measurements obtained using the patch-clamp technique on native membrane—the outer nuclear membrane of isolated *Xenopus* oocyte nuclei—as opposed to experiments using IP_3Rs reconstituted into planar lipid bilayers (Bezprozvanny *et al.*, 1991; Mak & Foskett, 1997; Mak *et al.*, 1998; Fraiman &

Dawson, 2004).

Because intracellular Ca^{2+} channels such as RyRs and IP_3Rs can be activated as well as inactivated by cytosolic Ca^{2+}, the effect of Ca^{2+} released by open intracellular Ca^{2+} channels on subsequent channel gating is presumably dependent on the details of single channel kinetics and difficult to predict *a priori*. Borrowing terminology from the literature on presynaptic facilitation of neurotransmitter release that focuses on accumulation of free residual Ca^{2+} in the synaptic terminal (Zucker & Regehr, 2002; Matveev *et al.*, 2004), one might hypothesize that "residual Ca^{2+}" from prior openings of intracellular Ca^{2+} channels would increase the steady-state open probability of a channel activated by Ca^{2+}, but decrease the open probability of a Ca^{2+}-inactivated channel. As we will see below, this is indeed the case; however, in quantitative terms the influence of residual Ca^{2+} on channel gating depends on the time scale for Ca^{2+} domain formation and collapse compared to the characteristic time scale for Ca^{2+} channel gating. Furthermore, if a channel exhibits both fast Ca^{2+} activation and slower Ca^{2+} inactivation, as is the case for some IP_3R and RyR subtypes and many realistic intracellular Ca^{2+} channel models (De Young & Keizer, 1992; Atri *et al.*, 1993; Bezprozvanny & Ehrlich, 1994; Keizer & Levine, 1996; Tang *et al.*, 1995; Kaftan *et al.*, 1997; Smith & Keizer, 1998; Swillens *et al.*, 1998; Swillens *et al.*, 1999; Moraru *et al.*, 1999), the influence of Ca^{2+} feedback on channel gating is potentially dependent in a complicated manner on the details of channel kinetics.

In order to clarify the possible effect of residual Ca^{2+} on the stochastic gating of Ca^{2+}-regulated Ca^{2+} channels, we formulate a mathematical model of the phenomenon by coupling the stochastic gating of a single channel model to an ordinary differential equation for the time-dependent $[Ca^{2+}]$ in a restricted cytoplasmic compartment or, alternatively, a partial differential equation for the buffered diffusion of intracellular Ca^{2+} in a homogeneous isotropic cytosol. This formulation allows us to analyze how the steady-state open probability (p_{open}) of four different single channel models depends on the size of a Ca^{2+} domain—i.e, the maximum domain $[Ca^{2+}]$—as well as the time constant for domain formation and collapse. Although the mathematical and computational methods described here will ultimately be used to analyze the effect of residual Ca^{2+} on a relatively complex channel model—the well-known De Young-Keizer IP_3R model—we introduce the model formulation using two minimal models that exhibit Ca^{2+} activation and Ca^{2+} inactivation, respectively.

Some of these results have previously appeared in abstract form (Mazzag *et al.*, 2004).

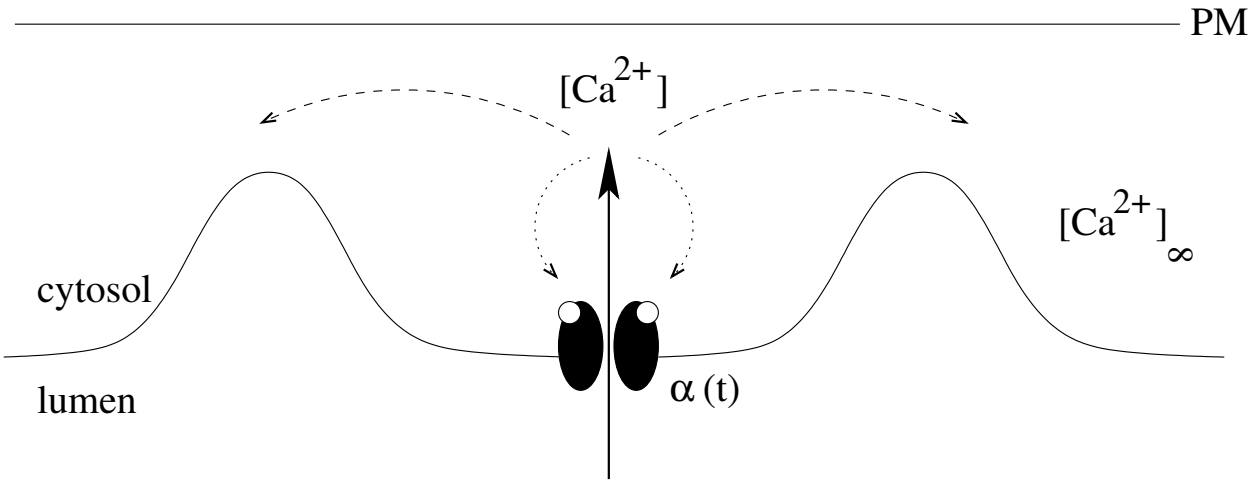

Figure 1: Schematic diagram showing the assumed relationship between the $[Ca^{2+}]$ in a restricted cytoplasmic compartment and cytosolic Ca^{2+}-regulatory sites (*open circles*) of a stochastically gating intracellular Ca^{2+} channel. *Dotted arrows* represent Ca^{2+} feedback on the channel. The time-dependent domain $[Ca^{2+}]$ satisfies Eq. 9 or Eq. 14: increases (*solid arrow*) at constant rate when the channel is open, and decreases (*dashed arrows*) at a rate proportional to the difference between the calcium concentration in the restricted compartment (denoted by $[Ca^{2+}]$ or c) and the bulk (denoted by $[Ca^{2+}]_\infty$ or c_∞).

2 Formulation of the Model

We study the effect of residual Ca^{2+} on the stochastic gating of Ca^{2+}-regulated Ca^{2+} channels by coupling a single-channel kinetic model of an ion channel of interest (see Section 2.1 and Section 2.2) to a mathematical model of the formation and collapse of the Ca^{2+} domain that is a consequence of—and may influence—channel gating (detailed in Section 2.3). Though the model formulation is completely general and can be used to analyze the effect of residual Ca^{2+} on arbitrarily complex single channel models, for clarity we begin with a comparatively simple case.

2.1 Two-state models of Ca^{2+}-regulated Ca^{2+} channels

Stochastic models of single channel gating often take the form of continuous-time discrete-state stochastic processes; for review see (Colquhoun & Hawkes, 1995; Smith, 2002*a*). For example, the transition-state diagram for a two-state channel activated by Ca^{2+} is

$$\text{(closed)}\quad C \underset{k^-}{\overset{k^+ c^\eta}{\rightleftharpoons}} O \quad \text{(open)} \tag{1}$$

where k^+c^η and k^- are transition rates with units of reciprocal time, k^+ is an association rate constant with units of $\text{conc}^{-\eta}\,\text{time}^{-1}$, η is the cooperativity of Ca^{2+} binding, and c is the local $[Ca^{2+}]$, that is, the $[Ca^{2+}]$ near a Ca^{2+}-regulatory site associated with the channel (see Fig. 1). The transition state diagram of the channel (Eq. 1) defines a discrete-state continuous-time stochastic process, $S(t)$, that takes on values in the state-space $\mathcal{S} = (C, O)$.

If the local $[Ca^{2+}]$ is constant, for example, equal to a fixed background $[Ca^{2+}]$ that we will denote by c_∞, Eq. 1 corresponds to the well-known telegraph process with an infinitesimal generator or Q-matrix given by (Colquhoun & Hawkes, 1995; Norris, 1997),

$$Q = (q_{ij}) = \begin{pmatrix} -k^+c^\eta & k^+c^\eta \\ k^- & -k^- \end{pmatrix}. \tag{2}$$

Note that the generator matrix can be decomposed as

$$Q = K_- + c^\eta K_+ = \begin{pmatrix} 0 & 0 \\ k^- & -k^- \end{pmatrix} + c^\eta \begin{pmatrix} -k^+ & k^+ \\ 0 & 0 \end{pmatrix}, \tag{3}$$

where the matrices K_- and K_+ involve the dissociation and association rate constants, respectively. The off-diagonal elements of the infinitesimal generator matrix give the probability per unit time of a transition from state i to state j,

$$q_{ij} = \lim_{\Delta t \to 0} \frac{\mathsf{P}\{S(t+\Delta t) = \mathcal{S}_j | S(t) = \mathcal{S}_i\}}{\Delta t} \qquad (i \neq j)\,,$$

while the diagonal elements are such that each row sum is zero, $\sum_j q_{ij} = 0$. In this study of the effect of residual Ca^{2+} on channel gating, the local $[Ca^{2+}]$ will generally not be given by the constant background $[Ca^{2+}]$ (c_∞) but will rather increase or decrease depending on whether the channel is open or closed (Fig. 1). Thus, although the stochastic process given by $S(t)$ and $c(t)$ has the Markov property—the future depends only on the present, not on the past—the Markov chain $S(t)$ is *time-inhomogeneous*, because transition rates involving local Ca^{2+} are not constant but rather functions of time (see Section 2.3).

While Eq. 1 shows a transition-state diagram for a two-state channel that is activated by Ca^{2+} binding to a Ca^{2+} regulatory site (Fig. 1), a two-state model that is *inactivated* by Ca^{2+} is given by,

$$\text{(open)}\quad O \underset{k^-}{\overset{k^+c^\eta}{\rightleftharpoons}} C \quad \text{(closed)}\ . \tag{4}$$

Notice that the generator matrix of this Ca^{2+}-inactivated channel model is also given by Eq. 2 if we reverse the order of the states: $S(t) \in \mathcal{S} = (1, 2) = (O, C)$. In order to distinguish the Ca^{2+} activated and Ca^{2+} inactivated models, it is necessary to define a column vector $\boldsymbol{u}_O$

that is 1 for open state(s) and 0 for closed states. Thus, $\boldsymbol{u}_O = (0,1)^T$ and the generator Eq. 3 together define a two-state model activated by Ca^{2+}, while $\boldsymbol{u}_O = (1,0)^T$ and Eq. 3 represent a Ca^{2+}-inactivated channel. Below we consider these minimal single channel models in some detail, as well as a significantly more complicated IP_3R model described below.

2.2 The De Young-Keizer IP_3R model

Many models of IP_3Rs have been published to date (De Young & Keizer, 1992; Atri *et al.*, 1993; Bezprozvanny & Ehrlich, 1994; Tang *et al.*, 1995; Kaftan *et al.*, 1997; Swillens *et al.*, 1998; Swillens *et al.*, 1998) most of which designed to reproduce various aspects of the single channel kinetics of the type 1 IP_3R, but see (LeBeau *et al.*, 1999; Sneyd & Dufour, 2002) for models of the IP_3R-2 and -3. In spite of their complexity, the infinitesimal generator matrices of these models can often be written as

$$Q = K_- + c^\eta K_+, \tag{5}$$

similar to the two-state case (Eq. 3). This notation is helpful because the Ca^{2+} dependence of a subset of transition rates is made explicit. To convince the reader of the generality of Eq. 5, we review the well-known De Young-Keizer IP_3R model and show that it can be put in this form.

Recall that the De Young-Keizer model views the IP_3R as a collection of n independent subunits, each of which has one binding site for inositol 1,4,5-trisphosphate (IP_3) and two binding sites for Ca^{2+} (De Young & Keizer, 1992). As shown in Fig. 2, three processes (IP_3-potentiation, Ca^{2+}-activation, and Ca^{2+}-inactivation) produce eight possible states for each IP_3R subunit. After assuming certain symmetries in the rate constants—e.g., the association rate constant (a_5) for Ca^{2+} binding to the activating site is the same whether the subunit is in state S_0, S_1, S_4, or S_5—and satisfying one remaining thermodynamic constraint ($d_1 d_2 = d_3 d_4$), De Young and Keizer chose parameters for their model IP_3R to fit three experimental observations; first, the Ca^{2+}-dependent dissociation constant of IP_3 binding to the IP_3R (Joseph *et al.*, 1989); second, the bell-shaped equilibrium open probability curve of the type 1 IP_3R as a function of $[Ca^{2+}]$ (Bezprozvanny *et al.*, 1991); and third, the rapidity of Ca^{2+}-activation compared to Ca^{2+}-inactivation (Parker & Ivorra, 1990).

When deriving the generator matrix for the De Young-Keizer model, we must keep in mind that the IP_3R model is only open when *all* of the n subunits are in the permissive state (S_6). In the present context, this means that the n IP_3R subunits are no longer *independent*, that is, the $[Ca^{2+}]$ experienced by each model IP_3R subunit depends on the state of the other $n-1$ subunits. In order to account for this subunit inter-dependence caused by

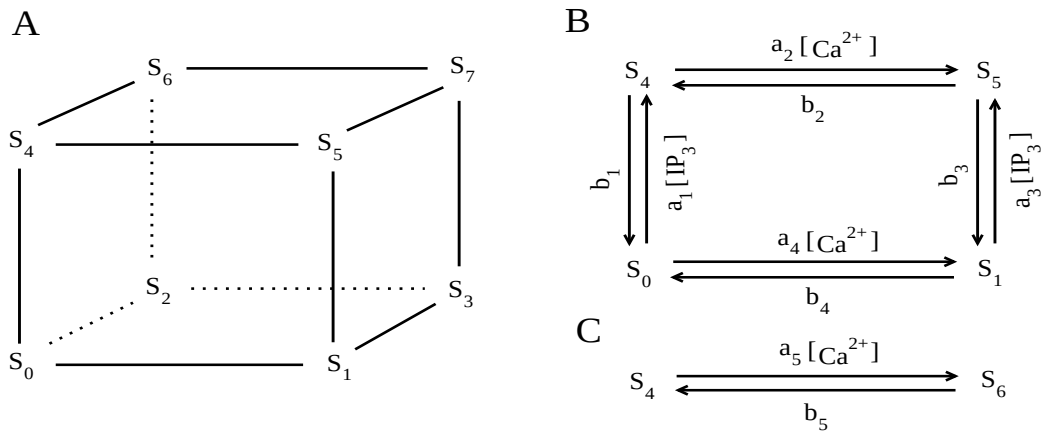

Figure 2: Transition-state diagram of one subunit of the De Young-Keizer IP_3R model (De Young & Keizer, 1992). A: The processes of Ca^{2+}-activation, Ca^{2+}-inactivation, and potentiation by IP_3 result in eight possible states (S_0–S_7) for each IP_3R subunit. B: The kinetics on both the front and back face of the cubic transition-state diagram in A. C: The kinetics of Ca^{2+} activation for the $S_4 \rightleftharpoons S_6$ transition. The same kinetics apply for the $S_5 \rightleftharpoons S_7$, $S_0 \rightleftharpoons S_2$, and $S_1 \rightleftharpoons S_3$ transitions. The channel is open when all four subunits of the model IP_3R are in the permissive state, S_6. The dissociation constants for each bimolecular reaction are given by $d_i = b_i/a_i$. See Table 1 for parameters.

Ca^{2+} domain-mediated inactivation, the De Young-Keizer transition-state diagram must be expanded to represent IP_3-potentiation, Ca^{2+}-activation, and Ca^{2+}-inactivation *for an entire channel*—i.e., all n subunits—as opposed to one subunit as shown in Fig. 2.

To derive the expanded generator matrix for the De Young-Keizer IP_3R model, we begin by writing the state space for a single subunit as $\mathcal{S}^{(1)} = (0, 1, \cdots, 7) = (S_0, S_1, \cdots, S_7)$ with the indicator of open states given by $\boldsymbol{u}_O^{(1)} = (0, 0, 0, 0, 0, 0, 1, 0)^T$ because state 6 is permissive. Assuming constant $[IP_3]$, the transition-state diagram for a single subunit of the De Young-Keizer IP_3R corresponds to an 8×8 generator matrix that takes the form

$Q^{(1)} = K_-^{(1)} + cK_+^{(1)}$, that is,

$$Q^{(1)} = \begin{pmatrix} \diamond & \cdot & \cdot & \cdot & a_1 i & \cdot & \cdot & \cdot \\ b_4 & \diamond & \cdot & \cdot & \cdot & a_3 i & \cdot & \cdot \\ b_5 & \cdot & \diamond & \cdot & \cdot & \cdot & a_1 i & \cdot \\ \cdot & b_5 & b_4 & \diamond & \cdot & \cdot & \cdot & a_3 i \\ b_1 & \cdot & \cdot & \cdot & \diamond & \cdot & \cdot & \cdot \\ \cdot & b_3 & \cdot & \cdot & b_2 & \diamond & \cdot & \cdot \\ \cdot & \cdot & b_1 & \cdot & b_5 & \cdot & \diamond & \cdot \\ \cdot & \cdot & \cdot & b_3 & \cdot & b_5 & b_2 & \diamond \end{pmatrix} + c \begin{pmatrix} \diamond & a_4 & a_5 & \cdot & \cdot & \cdot & \cdot & \cdot \\ \cdot & \diamond & \cdot & a_5 & \cdot & \cdot & \cdot & \cdot \\ \cdot & \cdot & \diamond & a_4 & \cdot & \cdot & \cdot & \cdot \\ \cdot & \cdot & \cdot & \diamond & \cdot & \cdot & \cdot & \cdot \\ \cdot & \cdot & \cdot & \cdot & \diamond & a_2 & a_5 & \cdot \\ \cdot & \cdot & \cdot & \cdot & \cdot & \diamond & \cdot & a_5 \\ \cdot & \cdot & \cdot & \cdot & \cdot & \cdot & \diamond & a_2 \\ \cdot & \cdot & \cdot & \cdot & \cdot & \cdot & \cdot & \diamond \end{pmatrix} \tag{6}$$

where $i = [\mathrm{IP}_3]$, $c = [\mathrm{Ca}^{2+}]$, a $\diamond$ indicates an element leading to row sum of zero, and the superscripted (1)'s indicate that these matrices represent the stochastic gating of a *single* subunit.

The De Young-Keizer $\mathrm{IP}_3\mathrm{R}$ model is composed of n identical subunits, each of which defined by Eq. 6, and all must be permissive (S_6) for the channel as a whole to be open. Assuming $n = 4$ subunits, this implies $8^4 = 4096$ channel states that can be arranged lexicographically as follows,

$$\mathcal{S}^{(4)} = ((0,0,0,0), (0,0,0,1), \cdots, (0,0,1,0), \cdots, (7,7,7,6), (7,7,7,7)).$$

Here the states 1, 2, 9, 4095, and 4096 are shown. The open state $(6,6,6,6)$ is state number 3511, because $6 \cdot 512 + 6 \cdot 64 + 6 \cdot 8 + 6 = 3510$. Using Kronecker products and sums (Steeb, 1997), the $8^4 \times 8^4$ generator matrix for the channel as a collective entity can be compactly written,

$$\begin{aligned} Q^{(4)} &= Q^{(1)} \oplus Q^{(1)} \oplus Q^{(1)} \oplus Q^{(1)} && (7) \\ &= Q^{(1)} \otimes I^{(3)} + I^{(1)} \otimes Q^{(1)} \otimes I^{(2)} + I^{(2)} \otimes Q^{(1)} \otimes I^{(1)} + I^{(3)} \otimes Q^{(1)} && (8) \end{aligned}$$

where $I^{(1)}$ is the the 8×8 identity matrix—i.e., the same size as $Q^{(1)}$—$I^{(2)}$ is $8^2 \times 8^2$, and $I^{(3)}$ is $8^3 \times 8^3$. Using $Q^{(1)} = K_-^{(1)} + cK_+^{(1)}$ and elementary properties of the Kronecker product we see that the generator matrix for the De Young-Keizer $\mathrm{IP}_3\mathrm{R}$ can be written as,

$$Q^{(4)} = K_-^{(4)} + cK_+^{(4)}$$

where $K_-^{(4)} = K_-^{(1)} \oplus K_-^{(1)} \oplus K_-^{(1)} \oplus K_-^{(1)}$ and similarly for $K_+^{(4)}$. Thus, we have shown that for fixed $[\mathrm{IP}_3]$ the De Young-Keizer model can in fact be written in the form of Eq. 5.

Because the 4 subunits of the De Young-Keizer $\mathrm{IP}_3\mathrm{R}$ model are identical, many of the 4096 states mentioned above are indistinguishable. Consequently, it is convenient to construct an

infinitesimal generator for this model using a reduced state space $\hat{\mathcal{S}}^{(4)}$ with each element taking the form

$$\hat{\mathcal{S}}_i^{(4)} = (n_0, n_1, \cdots, n_7) \qquad \text{where} \qquad \sum_i n_i = 4$$

and the n_i indicate the number of subunits (between 0 and 4) that are in state $\mathcal{S}_i^{(1)}$, that is, one of the eight subunit states shown in Fig. 2. An anti-lexicographical ordering of this reduced state space is (Nguyen *et al.*, 2004),

$$\begin{aligned}\hat{\mathcal{S}}^{(4)} \;=\; & ((4,0,0,0,0,0,0,0)\,,\ (3,1,0,0,0,0,0,0)\,,(3,0,1,0,0,0,0,0)\,,\cdots\,,\\ & (3,0,0,0,0,0,0,1)\,,\cdots\,,(2,2,0,0,0,0,0,0)\,,(0,0,0,0,0,0,3,1)\,,(0,0,0,0,0,0,0,4))\,.\end{aligned}$$

One may determine by enumeration that there are 330 elements in $\hat{\mathcal{S}}^{(4)}$, corresponding to the number of ways that four identical subunits can be assigned to eight states (or four indistinguishable balls placed in eight bins). This can be quickly confirmed as 330 is "$n + m - 1$ choose n" where $n = 4$ (the number of subunits/balls) $m = 8$ (the number of states/bins). Enumerating these 330 states anti-lexicographically one finds that the open state of the De Young-Keizer IP_3R model is state $326 = (0,0,0,0,0,0,4,0)$. Next, the 330×330 matrices K_- and K_+ (Eq. 5) are calculated element-by-element consistent with the transition rates of the single subunit (Eq. 6). For example, the 326th row of the generator matrix for the De Young-Keizer IP_3R model has nonzero elements representing transitions from state $(0,0,0,0,0,0,4,0) = 326$ to three destination states: $257 = (0,0,1,0,0,0,3,0)$, $312 = (0,0,0,0,1,0,3,0)$, and $327 = (0,0,0,0,0,0,3,1)$. These transition rates are $4b_1$, $4b_5$, and $4a_2c$, respectively, corresponding to one of the four subunits in state 6 making a transition into state 2, 4, or 7. This process is automated using a special purpose Matlab script (MathWorks, Inc.) that constructs the generator matrix of the 330-state De Young-Keizer IP_3R model (Eq. 5) from the 8-state subunit model (Eq. 6).

— ◇ ◇ ◇ —

In this paper we study the effect of residual Ca^{2+} on Ca^{2+}-regulated Ca^{2+} channels with generator matrices that take the form of Eq. 5. While not strictly required, for simplicity we assume that the cooperativity of Ca^{2+} binding (η) is the same for all transitions involving Ca^{2+} (usually $\eta = 1$). Thus, throughout this manuscript a single channel model is defined by the matrices giving the dissociation (K_-) and association (K_+) rate constants as well as the cooperativity of Ca^{2+} binding (η) and column vector indicating open states ($\boldsymbol{u}_O$). This is a reasonable starting point, because the generator matrices defining both minimal (Section 2.1) and realistic (Section 2.2) single channel models can be written in this form.

2.3 Two representations of the time-dependent Ca^{2+} domain

We study the effect of residual Ca^{2+} on Ca^{2+}-regulated Ca^{2+} channel models by coupling the stochastic gating of a single channel model to an ordinary differential equation for the time-dependent $[Ca^{2+}]$ in a restricted cytoplasmic compartment or, alternatively, a partial differential equation for the buffered diffusion of intracellular Ca^{2+} in a homogeneous isotropic cytosol.

Figure 1 shows the assumed relationship between the Ca^{2+}-regulatory sites of a stochastically gating intracellular Ca^{2+} channel and the time-dependent $[Ca^{2+}]$ in the case of a restricted cytoplasmic compartment. When the channel is open, the Ca^{2+} concentration—denoted by $[Ca^{2+}]$ or c—is assumed to increase (*solid arrow*) at constant rate. When the channel is closed, $[Ca^{2+}]$ decreases (*dashed arrows*) at a rate proportional to the concentration difference between the restricted compartment and the bulk $[Ca^{2+}]$—denoted by $[Ca^{2+}]_\infty$ or c_∞. The ordinary differential equation for domain $[Ca^{2+}]$ is thus

$$\frac{dc}{dt} = \alpha(t) - \frac{c - c_\infty}{\tau} \qquad \text{where} \qquad \alpha(t) = \begin{cases} 0 & \text{when} \quad S(t) = C \\ \alpha_0 & \text{when} \quad S(t) = O. \end{cases} \tag{9}$$

Here α_0 has units of conc/time and is proportional to the source amplitude of the channel and inversely proportional to the volume of the restricted compartment. From this expression, it is clear that the domain $[Ca^{2+}]$ (c) fluctuates between the minimum value c_∞ and a maximum of

$$c_{ss} = \tau\alpha_0 + c_\infty. \tag{10}$$

The parameter τ in Eq. 9 will be referred to as the time constant for Ca^{2+} domain formation and collapse or simply the "domain time constant." The value of τ is determined by the geometry of a problem of interest and characterizes the time required for Ca^{2+} to diffuse from the restricted domain to the bulk. For small values of τ, increases and decreases in $[Ca^{2+}]$ occur quickly each time there is a $C \to O$ or $O \to C$ transition in the single channel model, while for large values of τ changes in $[Ca^{2+}]$ occur more slowly. If the $[Ca^{2+}]$ is given by c_0 at time $t = t_0$, we see by integrating Eq. 9 that until a state transition occurs,

$$c\,(t) = \tilde{c} + (c_0 - \tilde{c})\, e^{-(t-t_0)/\tau} \tag{11}$$

where $\tilde{c}$ is the steady-state $[Ca^{2+}]$ for the current state of the channel, either c_∞ or $c_{ss} = \tau\alpha_0 + c_\infty$ for a closed or open channel, respectively.

— ◇ ◇ ◇ —

Ca^{2+} domains associated with Ca^{2+} channels are often modeled using reaction-diffusion equations where the channel is viewed as a point source for free Ca^{2+} in a homogeneous isotropic cytosol (Wagner & Keizer, 1994; Smith, 2000; Smith *et al.*, 2001). Under the assumptions of a single exogenous or endogenous Ca^{2+} buffer undergoing bimolecular association with Ca^{2+},

$$\mathrm{Ca^{2+}} + \mathrm{B} \underset{k_{off}^{buf}}{\overset{k_{on}^{buf}}{\rightleftharpoons}} \mathrm{CaB},$$

and equal diffusion coefficients for the free and bound form of the Ca^{2+} buffer, the relevant nonlinear reaction-diffusion equations are

$$\frac{\partial[\mathrm{Ca^{2+}}]}{\partial t} = D_c \nabla^2 [\mathrm{Ca^{2+}}] - R \qquad \frac{\partial[\mathrm{CaB}]}{\partial t} = D_b \nabla^2 [\mathrm{CaB}] + R \tag{12}$$

where the reaction terms are $R = k_{on}^{buf}[\mathrm{Ca^{2+}}][\mathrm{B}] - k_{off}^{buf}[\mathrm{CaB}]$ and the Ca^{2+}-bound buffer concentration is $[\mathrm{CaB}] = [\mathrm{B}]_\mathrm{T} - [\mathrm{B}]$ with $[\mathrm{B}]_\mathrm{T}$ indicating the total buffer concentration that is assumed to be initially spatially uniform and therefore constant. If the Ca^{2+} channel is modeled as a point source at the origin ($r = 0$) of a spherical polar coordinate system, the above assumptions imply (hemi)spherical symmetry and the Laplacian can be written

$$\nabla^2 = \frac{1}{r^2}\frac{\partial}{\partial r}\left[r^2 \frac{\partial}{\partial r}\right].$$

We also assume that far from the channel Ca^{2+} and buffer are in equilibrium so that the associated boundary conditions are,

$$\begin{aligned}
\lim_{r\to 0}\left\{-2\pi r^2 D_c \frac{\partial[\mathrm{Ca^{2+}}]}{\partial r}\right\} &= \sigma(t) \qquad \lim_{r\to\infty}[\mathrm{Ca^{2+}}] = [\mathrm{Ca^{2+}}]_\infty \\
\lim_{r\to 0}\left\{-2\pi r^2 D_b \frac{\partial[\mathrm{CaB}]}{\partial r}\right\} &= 0 \qquad \lim_{r\to\infty}[\mathrm{CaB}] = [\mathrm{CaB}]_\infty = \frac{[\mathrm{Ca^{2+}}]_\infty [\mathrm{B}]_\mathrm{T}}{[\mathrm{Ca^{2+}}]_\infty + K^{buf}}
\end{aligned}$$

where $\sigma(t)$ is the source amplitude of the Ca^{2+} channel (e.g, in units of μmoles/sec) and $K^{buf} = k_{off}^{buf}/k_{on}^{buf}$ is the dissociation constant of the Ca^{2+} buffer.

For simplicity, we further assume that the source amplitude is sufficiently weak and the total buffer concentration sufficiently high so that the homogeneous and isotropic cytosol is in the "excess buffer limit" (Neher, 1986; Naraghi & Neher, 1997; Smith *et al.*, 2001). Under these conditions the free and bound buffer concentrations are well-approximated by their equilibrium values even near the source—that is, $[\mathrm{CaB}](r,t) \approx [\mathrm{CaB}]_\infty$ and $[\mathrm{B}](r,t) \approx [\mathrm{B}]_\infty$—and the $[\mathrm{Ca^{2+}}]$ near the channel satisfies the the cable equation,

$$\frac{\partial[\mathrm{Ca^{2+}}]}{\partial t} = D_c \nabla^2 [\mathrm{Ca^{2+}}] - \frac{[\mathrm{Ca^{2+}}] - [\mathrm{Ca^{2+}}]_\infty}{\theta}.$$

In this equation, D_c is the free Ca^{2+} diffusion coefficient and θ is the time constant of the medium given by

$$\theta = \frac{1}{k_{on}^{buf}[\mathrm{B}]_\infty} \qquad \text{where} \qquad [\mathrm{B}]_\infty = [\mathrm{B}]_\mathrm{T} - [\mathrm{CaB}]_\infty = \frac{K^{buf}[\mathrm{B}]_\mathrm{T}}{[\mathrm{Ca}^{2+}]_\infty + K^{buf}}. \tag{13}$$

The diffusion coefficient D_c and time constant θ together imply a length scale of $\lambda = \sqrt{D_c\theta}$. In the excess buffer limit, the time constant θ depends on both the buffer association rate and the free buffer concentration far from the source. While admittedly the excess buffer limit is assumed largely for convenience, the range of validity of this approximation is well understood (Neher, 1998; Smith *et al.*, 2001). In systems where the channel source amplitude is great enough to saturate cytosolic Ca^{2+} buffers, the excess buffer limit can be obtained upon addition of exogenous buffers such as EGTA. For example, using $k_{on}^{buf} = 1.5\ \mu\mathrm{M}^{-1}\mathrm{s}^{-1}$, $k_{off}^{buf} = 0.3\ \mathrm{s}^{-1}$, $[\mathrm{B}]_\mathrm{T} = 1000\ \mu$M, $D_b = 113\ \mu\mathrm{m}^2/\mathrm{s}$ for EGTA, $D_c = 250\ \mu\mathrm{m}^2/\mathrm{s}$, and i_{Ca}= 0.05 pA, the dimensionless diffusion coefficients for free Ca^{2+} and buffer,

$$\varepsilon_c = \frac{(2\pi)^2 D_c^3 \left(K^{buf}\right)^2}{\sigma^2 k_{on}^{buf}[\mathrm{B}]_\mathrm{T}} \qquad \varepsilon_b = \frac{(2\pi)^2 D_c^2 D_b K^{buf}}{\sigma^2 k_{on}^{buf}},$$

evaluate to $\epsilon_c = 0.245$ and $\epsilon_b = 554$, well within the excess buffer regime (see Fig. 9.1 and Eqs. 4.4 and 4.5 in (Smith *et al.*, 2001)).

Thus, to study the effect of residual Ca^{2+} on channel models coupled to a homogeneous isotropic cytosol we use a finite difference scheme to numerically solve

$$\frac{\partial c}{\partial t} = D_c\nabla^2 c - \frac{c - c_\infty}{\theta} \qquad \lim_{r\to 0}\left\{-2\pi r^2 D_c \frac{\partial c}{\partial r}\right\} = \sigma(t) \qquad \lim_{r\to\infty} c = c_\infty \tag{14}$$

where the $\sigma(t)$ that occurs in Eq. 14 is analogous to the term $\alpha(t)$ in Eq. 9 and is a function of the state of the stochastically gating ion channel,

$$\sigma(t) = \begin{cases} 0 & \text{when} \quad S(t) = C \\ \sigma_0 & \text{when} \quad S(t) = O. \end{cases} \tag{15}$$

The source amplitude of the open channel σ_0 is proportional to the unitary current (i_{Ca}) via $\sigma_0 = i_{Ca}/zF$ where $z = 2$ is the valence of Ca^{2+} and F is Faraday's constant. Because here the domain $[Ca^{2+}]$ is a function of both space and time, the $[Ca^{2+}]$ used in the generator matrix (Eq. 5) of the stochastically gating ion channel is the $[Ca^{2+}]$ given by Eq. 14 evaluated at a fixed distance r_0 from the channel pore, $c(r = r_0, t)$. If the Ca^{2+}-regulation is direct and does not involve accessory proteins, this distance r_0 is presumably short and r_0/λ is a small dimensionless parameter.

— ◇ ◇ ◇ —

In summary, we study the effect of residual Ca^{2+} on Ca^{2+}-regulated Ca^{2+} channels by coupling a single-channel model to a time-dependent Ca^{2+} domain. The single channel model specified by K_-, K_+, and $\boldsymbol{u}_O$ includes a number of parameters—the non-zero off-diagonal entries of K_- and K_+. In the case of a restricted cytoplasmic compartment, there are 3 additional parameters: τ, α_0, c_∞, and the auxiliary parameter c_{ss} given by Eq. 10. In the case of a homogeneous isotropic cytosol there are 5 additional parameters: θ, λ, σ_0, r_0, and c_∞. Here the maximum $[Ca^{2+}]$ experienced by the Ca^{2+}-regulatory site of the channel is

$$c_{ss} = \frac{\sigma_0}{2\pi D_c r_0} e^{-r_0/\lambda} + c_\infty \qquad \text{where} \qquad \lambda = \sqrt{\theta D_c}. \tag{16}$$

For example, using the parameters for millimolar EGTA above and a distance between channel pore and Ca^{2+} binding site of $r_0 = 0.021$ μm, the maximum domain $[Ca^{2+}]$ (c_{ss}) for a 0.066 pA channel is approximately 10 μM. Note that in the case of the homogeneous isotropic cytosol assuming the excess buffer approximation results in reaction terms that are similar to the restricted cytosolic compartment case (cf. Eq. 14 and Eq. 9). Thus, we might expect similar results obtained using these two distinct representations of the time-dependent Ca^{2+} domain.

2.4 Monte Carlo Simulation Method

Simulation of a Ca^{2+} channel coupled a dynamic Ca^{2+} domain is straightforward and utilizes a numerical scheme for the time-evolution of the $[Ca^{2+}]$ as well as a numerical scheme that produces an instantiation of the time-inhomogeneous stochastic process representing channel gating. Because the simplest algorithms for simulating channel gating are first order accurate in time, we used Euler's method to integrate Eq. 9. The numerical schemes used to solve Eq. 14 followed previous work (Smith *et al.*, 1996; Smith, 1996).

For a review of Monte Carlo simulation methods applicable to stochastically gating ion channel models see (Colquhoun & Hawkes, 1995; Smith, 2002*a*). Briefly, time is discretized and at each time-step the channel is given an opportunity to change state. In a short time interval of length Δt, the probability that the channel makes a transition between state i and j is given by the elements of

$$W = (w_{ij}) = I + Q\Delta t \tag{17}$$

where I is a commensurate identity matrix, that is,

$$w_{ij} = \mathsf{P}\{S(t) = \mathcal{S}_i, t + \Delta t | S(t) = \mathcal{S}_i, t\}$$

for sufficiently small Δt. Because Q is a function of the time-dependent domain $[Ca^{2+}]$, the row of W corresponding to the current state needs to be calculated at every time step. The

non-zero entries of this row will always sum to one and can be used to partition the unit interval. Next, a pseudo-random number generator produces a random variable uniformly distributed on [0,1] and the transition from state i to j occurs if the random number falls on the partition associated with column j of W. We chose Δt small enough so that the diagonal entries of W are greater than 0.9 when the $[Ca^{2+}]$ is it's maximum value ($c = c_{ss}$); thus, most time-steps do not result in a state change for the channel. For example, for the two-state channel with generator given by Eq. 2, the transition probability matrix W defined by Eq. 17 is

$$W = \begin{pmatrix} \mathsf{P}\{C, t+\Delta t|C,t\} & \mathsf{P}\{O, t+\Delta t|C,t\} \\ \mathsf{P}\{C, t+\Delta t|O,t\} & \mathsf{P}\{O, t+\Delta t|O,t\} \end{pmatrix} = \begin{pmatrix} 1-k^+c(t)^\eta\Delta t & k^+c(t)^\eta\Delta t \\ k^-\Delta t & 1-k^-\Delta t \end{pmatrix}.$$

In this case Δt would be chosen to satisfy $\Delta t < 0.1/\max(k^+c_{ss}^\eta, k^-)$.

This Monte Carlo simulation method generalizes readily when channel models with more states are used (Colquhoun & Hawkes, 1995; Smith, 2002*a*). Appendix A presents an exact simulation method applicable to the case of a restricted cytoplasmic compartment (Eq. 9).

3 Results

3.1 Monte-Carlo simulation of the effect of residual Ca^{2+} on two-state channels

In order to clarify how changes in the observed open probability (p_{open}) may be a function of the the source amplitude of the open channel (α_0) and the time constant (τ) for Ca^{2+} domain formation and collapse in a restricted cytoplasmic compartment, we analyze the two-state models described above, one of which is activated by Ca^{2+} (Eq. 1), and the other inactivated by Ca^{2+} (Eq. 4). In this section we assume a spatially restricted cytosolic compartment and model the the dynamics of the time-dependent Ca^{2+} domain using Eq. 9.

Figure 3 shows representative Monte Carlo simulations of the two-state Ca^{2+}-activated channel (Eq. 1). When the channel is not conducting Ca^{2+} ($\alpha_0 = 0$), but rather gating in the presence of a constant background $[Ca^{2+}]$ of $c_\infty = 0.1$ μM, these parameters imply an equilibrium open probability of $p_{open} = 0.17$. The general expression for p_{open} under these conditions,

$$p_{open} = \frac{C \to O}{C \to O + C \leftarrow O} = \frac{k^+c_\infty^\eta}{k^+c_\infty^\eta + k^-} = \frac{c_\infty^\eta}{c_\infty^\eta + K^\eta}, \tag{18}$$

can be found algebraically or, as indicated by the first equality, using a diagrammatic approach; for review see (Hill, 1977). Here the cooperativity of Ca^{2+} binding is $\eta = 1$ and

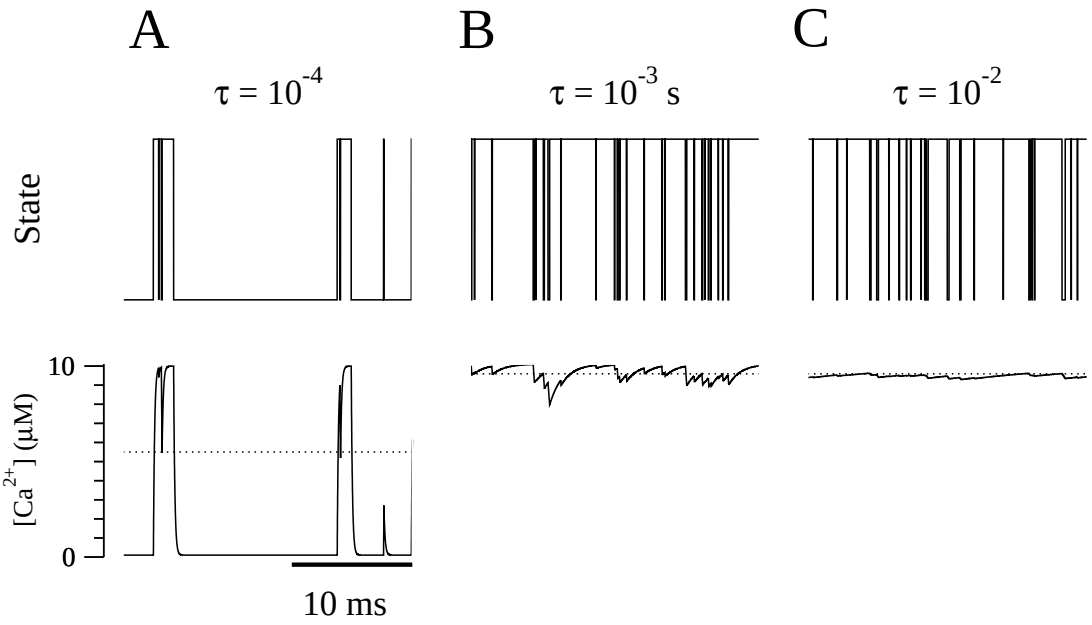

Figure 3: Monte Carlo simulations of a Ca^{2+}-activated channel using different time constants (τ) for Ca^{2+} domain formation and collapse in a restricted cytoplasmic compartment. A: $\tau = 10^{-4}$ s, a comparatively fast Ca^{2+} domain. B: $\tau = 10^{-3}$ s, intermediate. C: $\tau = 10^{-2}$ s, slow. The *dotted line* denotes the average $[Ca^{2+}]$ over the last 250 ms of a 1 sec simulation (5.5, 9.5, and 9.5 μM, respectively). Parameters: $\eta = 1$, $k^+ = 2\ \mu\text{M}^{-1}\text{ms}^{-1}$ and $k^- = 1\ \text{ms}^{-1}$.

the rate constants $k^+ = 2\ \mu\text{M}^{-1}\text{ms}^{-1}$ and $k^- = 1\ \text{ms}^{-1}$ lead to a dissociation constant of $K = 0.5\ \mu$M. When a channel is conducting Ca^{2+} ($\alpha_0 > 0$), its stochastic gating occurs in the presence of a time-dependent Ca^{2+} domain with concentration in the range $c_\infty \le [Ca^{2+}] \le c_{ss} = \tau\alpha_0 + c_\infty$. Comparing the columns of Fig. 3, we see that for small τ the domain $[Ca^{2+}]$ increases and decreases quickly (A), for large τ the domain fluctuates more slowly (B and C), and that p_{open} dramatically increases as the domain time constant increases from $\tau = 10^{-4}$ to 10^{-3} s (A to B). This range of τ is consistent with theoretical and experimental results indicating that domain $[Ca^{2+}]$ may change by tens of micromolar in a millisecond (Smith *et al.*, 1998; Thul & Falcke, 2004). The three simulations in Fig. 3 use different source amplitude for the open channel (α_0) in order to focus on the effect of the domain time constant (τ) rather than the maximum domain $[Ca^{2+}]$ (c_{ss}). In each simulation, the value of α_0 is chosen so that the maximum $[Ca^{2+}]$ in the restricted cytoplasmic space is fixed at $c_{ss} = 10\ \mu$M, that is, $\alpha_0 = (c_{ss} - c_\infty)/\tau$ in Fig. 3A–C (see Eq. 10).

Figure 3 demonstrates that the effect of residual Ca^{2+} on a two-state Ca^{2+}-activated channel depends on the domain time constant (τ). After controlling for the domain size (c_{ss}),

we find that a slow Ca^{2+} domain promotes Ca^{2+} activation. We also find that increasing the source amplitude of the channel (α_0) while keeping the domain time constant fixed leads to increased p_{open} (not shown). A qualitative explanation of these effects of residual Ca^{2+} begins by noting that the $O \to C$ transition is unimolecular and does not depend on $[Ca^{2+}]$; consequently, the open dwell times are exponentially distributed with parameter and mean $1/k^-$. However, the $C \to O$ transitions are bimolecular and do depend on $[Ca^{2+}]$. Because this variable transition rate is always greater than or equal to the value obtained when the channel isn't conducting Ca^{2+}—$k^+c(t) \geq k^+c_\infty$—it is no surprise that p_{open} is an increasing function of α_0 (not shown). Furthermore, because this $C \to O$ transition rate $k^+c(t)$ *decreases* as the channel dwells in the closed state ($\tilde{c} = c_\infty$ in Eq. 11), a slow Ca^{2+} domain means that residual Ca^{2+} 'lingers' and promotes Ca^{2+}-dependent activation. This explanation of why p_{open} is an increasing function of the domain time constant is supported by the observation that the average $[Ca^{2+}]$ experienced by the channel is higher when the domain is slow (see *dotted lines* in Fig. 3).

— ◇ ◇ ◇ —

Intuitively, one might expect the situation to be reversed in the case of a two-state channel that is inactivated by Ca^{2+} (Eq. 4). However, the Monte Carlo simulations of Fig. 4 show that this is not the case. While it is true that increasing the source amplitude of the Ca^{2+}-inactivated channel leads to a decrease in p_{open} (not shown), after controlling for the domain size (c_{ss}) we observe that increased domain time constant leads to *increased* p_{open} (compare columns of Fig. 4). Though the overall increase in p_{open} is not as large, the direction of the effect of residual Ca^{2+} is not reversed but rather identical to that obtained for the two-state Ca^{2+}-activated channel (cf. Fig. 3). This counter-intuitive result can be explained by remembering that in the case of the Ca^{2+}-inactivated channel, it is the $C \to O$ transition that is unimolecular giving a mean *closed* dwell time of $1/k^-$. Conversely, the $O \to C$ transition is bimolecular and the transition rate $k^+c(t)$ *increases* as the channel dwells in the open state ($\tilde{c} = c_{ss}$ in Eq. 11), that is, for the Ca^{2+}-inactivated channel, a fast Ca^{2+} domain means that residual Ca^{2+} accumulates more quickly and promotes inactivation. Thus, relief from Ca^{2+}-inactivation as the domain time constant τ increases causes p_{open} to be slightly larger in Fig. 4C than Fig. 4A.

— ◇ ◇ ◇ —

Using channel parameters from Figs. 3 and 4, Fig. 5 summarizes a large number of Monte Carlo simulations of the two-state Ca^{2+}-activated and Ca^{2+}-inactivated channel models. The

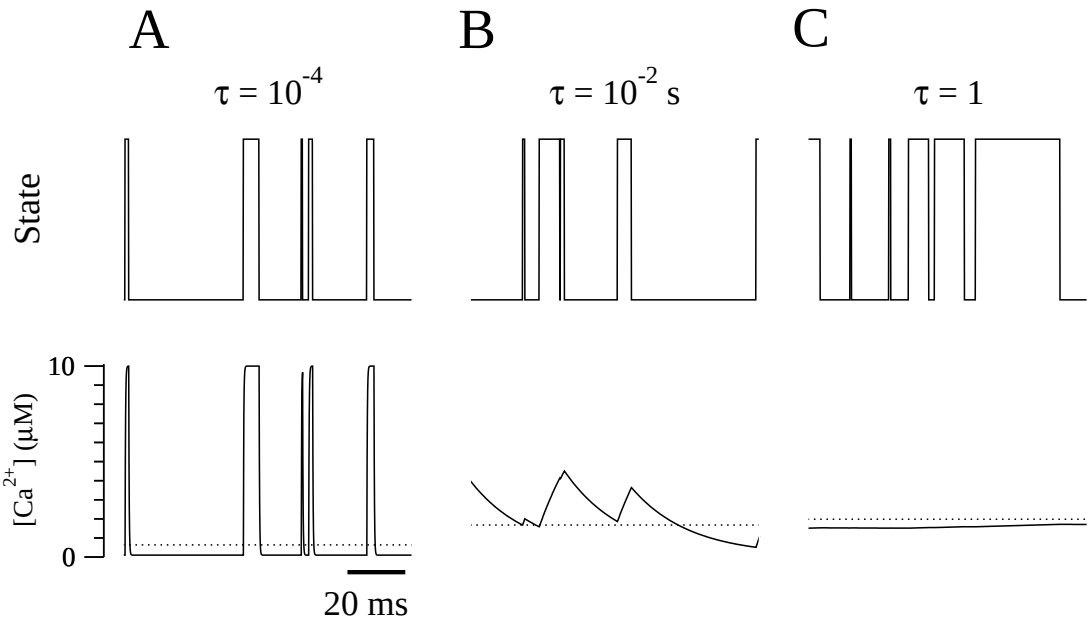

Figure 4: Monte Carlo simulations of a Ca^{2+}-inactivated channel using different time constants (τ) for Ca^{2+} domain formation and collapse in a restricted cytoplasmic compartment. A: $\tau = 10^{-4}$ s, a comparatively fast Ca^{2+} domain. B: $\tau = 10^{-2}$ s, intermediate. C: $\tau = 1$ s, slow. The *dotted line* denotes the average $[Ca^{2+}]$ over last 250 ms of a 1 sec simulation (0.6, 1.7, and 2.0 μM, respectively). Parameters: $\eta = 1$, $k^+ = 0.2$ $\mu M^{-1} ms^{-1}$ and $k^- = 0.1$ ms^{-1}.

filled circles in Fig. 5A and B show that when c_{ss} is fixed at 10 μM, p_{open} is a monotonic increasing function of the domain time constant (τ). This occurs regardless of whether the channel is activated or inactivated by Ca^{2+} (compare panels A and B). In the former case, residual Ca^{2+} of a slow domain decays more slowly leading to increased activation. In the later case, residual Ca^{2+} of a slow domain accumulates more slowly leading to relief from inactivation.

The *open squares* of Fig. 5 summarize a similar study in which the maximum domain concentration (c_{ss}) is not controlled. Instead, the source amplitude of the channel (α_0) is fixed and, as indicated by Eq. 10, this implies that changes in the domain time constant (τ) lead to corresponding changes in domain size (c_{ss}). Here we find that increasing τ and c_{ss} simultaneously leads to increased p_{open} in the case of the Ca^{2+}-activated channel and decreased p_{open} in the case of the Ca^{2+}-inactivated channel. Figure 5 also shows results obtained using methods detailed below that are consistent with the Monte Carlo simulations.

— ◇ ◇ ◇ —

To summarize, some Monte Carlo simulation results of two-state Ca^{2+}-activated and

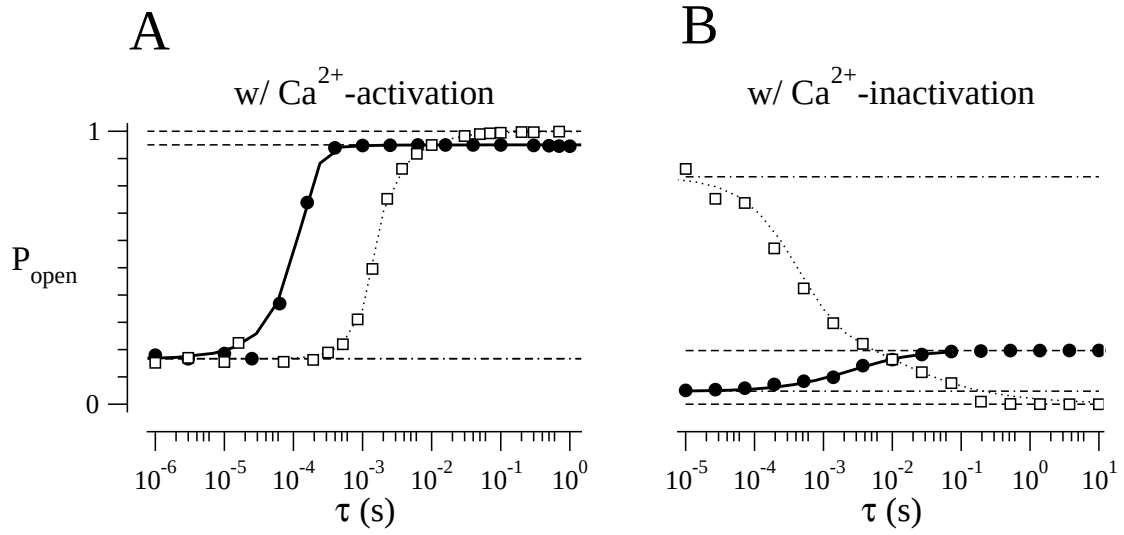

Figure 5: Summary of results of the effect of the domain time constant (τ) on the observed open probability (p_{open}) of the two-state Ca^{2+}-activated (A) and Ca^{2+}-inactivated (B) channels. Analytical estimates described in Section 3.2 giving p_{open} in the limit of small (*dot-dashed lines*) and large (*dashed lines*) τ agree with Monte Carlo (*filled circles* and *open squares*, Section 3.1) and probability density (*solid* and *dotted lines*, Section 3.3) simulation results using fixed domain size ($c_{ss} = 10$ μM, *solid lines* and *filled circles*) or fixed source amplitude ($\alpha_0 = 990$ μM/s, *dotted lines* and *open squares*). Channel gating parameters as Fig. 3 in panel A and Fig. 4 in panel B.

Ca^{2+}-inactivated models are quite intuitive; for example, the dependence of p_{open} on α_0 and the results obtained when τ is varied with fixed α_0. However, other results such as the dependence of p_{open} on τ for fixed c_{ss} are counter-intuitive. This suggests that it may be difficult to predict the effect of residual Ca^{2+} on the observed open probability of more complicated single channel models and motivates the development of a general biophysical theory for the phenomenon.

3.2 Analytical estimates of the effect of residual Ca^{2+} on two-state channels

An important aspect of the summary presented in Fig. 5 is that all four parameter studies give results that asymptotically approach fixed values in the limit of a fast (small τ) or slow (large τ) Ca^{2+} domain. Monte Carlo simulations show that p_{open} monotonically increases or decreases between these limiting values. In this section we estimate these limits, focusing again on the case where $c_{ss} = \alpha_0\tau + c_\infty$ remains fixed as τ is varied. We denote the limiting values of p_{open} as $\tau \to 0$ or ∞ as $\underline{p_{open}}$ and $\overline{p_{open}}$, respectively.

The values of τ for which these estimates are likely to be accurate can be established by considering the range of time constants associated with the channel. For both the Ca^{2+}-activated and Ca^{2+}-inactivated channel, one dwell time is constant ($1/k^-$) and the other variable ($1/k^+c(t)^\eta$ with $c_\infty \le c \le c_{ss}$). Using $\eta = 1$, $k^+ = 2\ \mu\text{M}^{-1}\text{ms}^{-1}$ and $k^- = 1\ \text{ms}^{-1}$, we find the time constants associated with channel gating are thus $1/k^- = 1$ ms and $1/k^+c_{ss}^\eta = 0.05$ ms through $1/k^+c_\infty^\eta = 5$ ms. The *broken lines* of Fig. 5 show that when the domain time constant τ is an order of magnitude smaller or larger than these values, p_{open} is well-approximated by either $\underline{p_{open}}$ or $\overline{p_{open}}$.

In the limit of fast domain formation and collapse (small τ), the periods of time when the $[Ca^{2+}]$ is changing become insignificant and the Ca^{2+} regulatory site of the channel is to good approximation exposed to the steady-state domain $[Ca^{2+}]$ associated with each state, that is, $[Ca^{2+}] \approx c_\infty$ when the channel is closed and $[Ca^{2+}] \approx c_{ss}$ when the channel is open. Because the Ca^{2+}-dependent transition of the two-state channel activated by Ca^{2+} originates from a closed state, $\underline{p_{open}}$ is in this case

$$\underline{p_{open}} = \left.\frac{C \to O}{C \to O + C \leftarrow O}\right|_{c=c_\infty} = \frac{k^+c_\infty^\eta}{k^+c_\infty^\eta + k^-} = \frac{c_\infty^\eta}{c_\infty^\eta + K^\eta}. \tag{19}$$

Using $c_\infty = 0.1\ \mu$M and the parameters of Fig. 3 we find $\underline{p_{open}} = 0.17$. For the two-state channel inactivated by Ca^{2+}, the Ca^{2+}-dependent transition originates from an open state and we find a different result,

$$\underline{p_{open}} = \left.\frac{O \leftarrow C}{O \leftarrow C + O \to C}\right|_{c=c_{ss}} = \frac{k^-}{k^- + k^+c_{ss}^\eta} = \frac{K^\eta}{c_{ss}^\eta + K^\eta}, \tag{20}$$

which using $c_{ss} = 10\ \mu$M gives $\underline{p_{open}} = 0.05$.

For the simulations where α_0 is held constant, the substitution $c_{ss} = \tau\alpha_0 + c_\infty$ is made before taking the limit $\tau \to 0$. When c_{ss} is not controlled and instead α_0 is fixed, the open probability for the Ca^{2+}-activated channel in the small τ limit remains $\underline{p_{open}} = 0.17$. However, for fixed α_0 the open probability for the Ca^{2+}-inactivated channel in the small τ limit is

$$\underline{p_{open}} = \lim_{\tau\to 0}\left\{\frac{K^\eta}{K^\eta + (\alpha_0\tau + c_\infty)^\eta}\right\} = \frac{K^\eta}{K^\eta + c_\infty^\eta},$$

or $\underline{p_{open}} = 0.83$.

All of the above estimates for $\underline{p_{open}}$ are consistent with the Monte Carlo simulations of Fig. 5 and are presented as *broken lines* in this figure. In Section 3.4 we show how this approach can be generalized to arbitrarily complex channel models.

— ◇ ◇ ◇ —

Estimating $\overline{p_{open}}$ in the case of a slow Ca^{2+} domain (large τ) is slightly more complicated. We begin by noticing for large values of τ in both Fig. 3 and Fig. 4 the $[Ca^{2+}]$ is nearly constant. We denote this unknown value by c_* and assume that for large τ the growth in $[Ca^{2+}]$ is proportional to the open probability of the channel so that c_* is given by

$$c_* = c_{ss}\overline{p_{open}} + c_\infty\,(1 - \overline{p_{open}}) \tag{21}$$

or $c_* = c_d p_{open} + c_\infty$ where $c_d = c_{ss} - c_\infty$ is the maximum increase in $[Ca^{2+}]$ above background experienced by the open channel. We surmise that $\overline{p_{open}}$ for the Ca^{2+}-activated channel in the case of a slow domain (large τ) is given by simultaneous solution of Eq. 21 and

$$\overline{p_{open}} = \frac{c_*^\eta}{c_*^\eta + K^\eta}. \tag{22}$$

Similarly, in the large τ limit $\overline{p_{open}}$ for the Ca^{2+}-inactivated channel is given by simultaneous solution of Eq. 21 and

$$\overline{p_{open}} = \frac{K^\eta}{c_*^\eta + K^\eta}. \tag{23}$$

These estimates for $\overline{p_{open}}$ are validated by their agreement with the results of Monte Carlo simulation (Fig. 5).

— ◇ ◇ ◇ —

The form of Eqs. 19–23 makes it clear that the dissociation constant K for Ca^{2+} binding to a two-state Ca^{2+} regulated Ca^{2+} channel determines the limiting open probability for very fast or slow Ca^{2+} domains. When the channel rate constants (k^+ and k^-) are both decreased by a factor of 10, this results in a log unit rightward shift of the p_{open} vs. τ curves, but the limiting values for a fast and slow domain do not change (not shown).

Figure 6 demonstrates the effect of changing the dissociation constant K by comparing p_{open} as a function of τ for both two-state models using $K = 0.5$ μM (as Fig. 5, *thin lines*) and $K = 5$ μM (*thick lines*, k^- increase ten-fold, k^+ unchanged). Regardless of whether c_{ss} or α_0 is fixed, this increased in the dissociation constant for Ca^{2+} binding causes p_{open} to decrease for the Ca^{2+}-activated channel and increase for the Ca^{2+}-inactivated channel. These observations—as well as the fact that the limiting values $\underline{p_{open}}$ and $\overline{p_{open}}$ either may or may not change—are all consistent with Eqs. 19–23.

Changes in the dissociation constant for Ca^{2+} binding to the two-state channel cause vertical shifts in the p_{open} vs. τ result. Similarly, changes in rate constants (for fixed K) leads to horizontal shift (not shown). However, neither parameter change influences the qualitative aspects of the effect of residual Ca^{2+} on two-state channels. The relationship between the limiting values $\underline{p_{open}}$ and $\overline{p_{open}}$ is not sensitive to the particular parameters

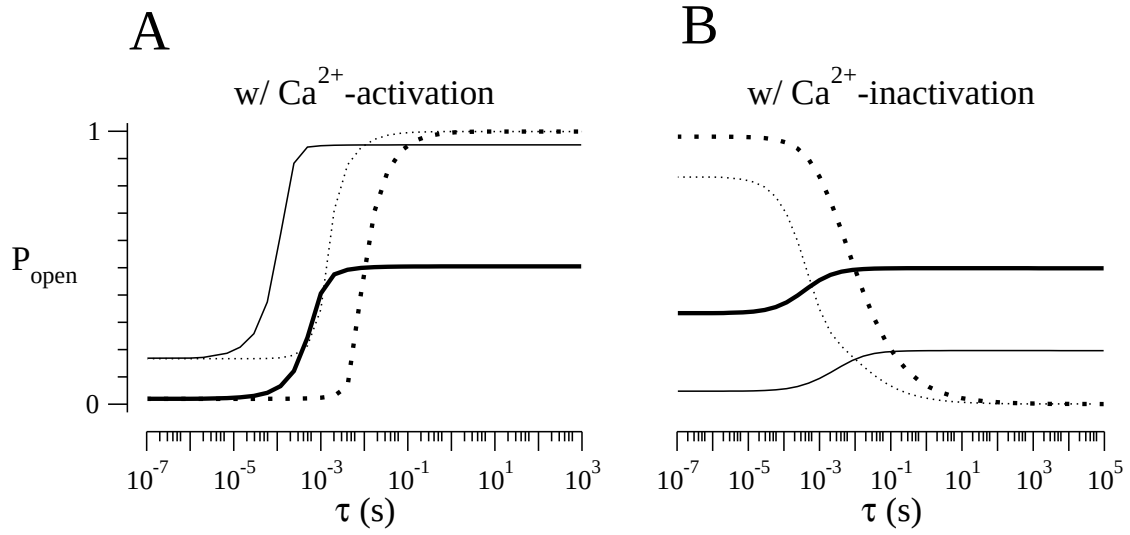

Figure 6: The effect of the domain time constant (τ) on the observed open probability (p_{open}) is qualitatively the same when the dissociation constant is increased from $K = 0.5$ μM (*thin lines*) where k^+ and k^- are as Fig. 5 to $K = 5$ μM (*thick lines* where k^- is increased 10-fold). Results are shown for both fixed domain size ($c_{ss} = 10$ μM, *solid lines*), and fixed source amplitude ($\alpha_0 = 990$ μM/s, *dotted lines*). The value of p_{open} in the small and large τ limits decreases with increasing K for the Ca^{2+}-activated channel (A) and increases for Ca^{2+}-inactivated channel (B). Calculations performed using the analytical methods discussed in Sections 3.2 and 3.3.

chosen for the channel kinetics. In the case of the Ca^{2+}-activated channel, for example, as long as η is an integer, $\underline{p_{open}} < \overline{p_{open}}$ for any k^- and k^+ (cf. Eqs. 19 and 22).

— ◇ ◇ ◇ —

Figure 7 shows a graphical method of estimating $\overline{p_{open}}$ in the large τ limit. The *dashed line* in Fig. 7A shows $\overline{p_{open}}$ of the Ca^{2+}-activated channel plotted as a function of the unknown c_*, while the *solid line* shows the linear dependence of c_* on possible values of $\overline{p_{open}}$ ranging from 0 to 1. The intersection of these two curves (*filled square*) corresponds to simultaneous solution of Eqs. 21 and 22. The *dotted line* in Fig. 7A shows $\overline{p_{open}}$ of the Ca^{2+}-inactivated channel and the equilibrium (*filled circle*) corresponding to solution of Eqs. 21 and 23. Figure 7B uses this graphical technique to make it clear that in the large τ limit there may be more than one solution pair ($\overline{p_{open}}$,c_*) for the two-state channel activated by Ca^{2+}. In fact, there are three equilibria using parameters of Fig. 3 when the cooperativity is increased to $\eta = 4$. Conversely, Fig. 7C shows that for the two-state channel inactivated by Ca^{2+} there can be only one equilibria.

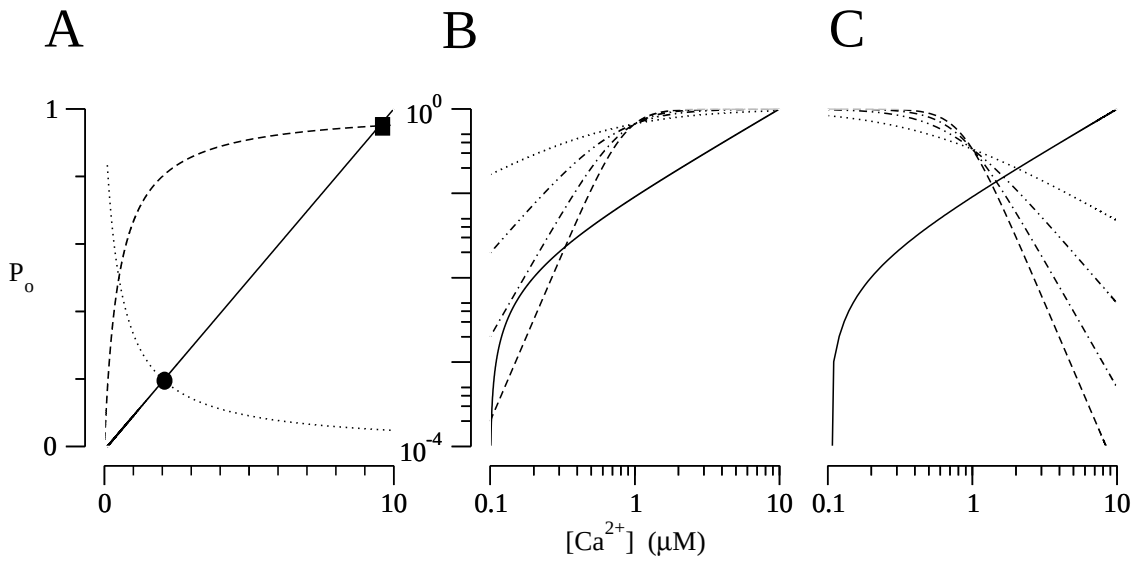

Figure 7: Graphical technique for estimating $\overline{p_{open}}$ of Ca^{2+}-regulated Ca^{2+} channels coupled to a slow Ca^{2+} domain. *Solid lines* plot the linear relationship between the unknown limiting $[Ca^{2+}]$ (c_*) and the equilibrium open probability assumed by Eq. 21. *Broken lines* plot $\overline{p_{open}}$ as a function of c_* as determined by the single channel model. Intersections represent stable or unstable equilibria. A: *Dashed* and *dotted lines* correspond to Ca^{2+}-activated (Eq. 22) and Ca^{2+}-inactivated (Eq. 23) channel, respectively. B,C: *Broken lines* show $\overline{p_{open}}$ for the Ca^{2+}-activated (B) and Ca^{2+}-inactivated (C) channel using different values of cooperativity of Ca^{2+} binding (η = 1, 2, 3, 4). Linear relationship between c_* and $\overline{p_{open}}$ (*solid lines*) is curved on log-log plot. Other parameters as Figs. 3 and 4.

Because a cooperativity of $\eta = 4$ may seem unrealistic, Fig. 8A presents a graphical analysis of the large τ limit for a two-state Ca^{2+}-activated channel with $\eta = 2$ (see legend for rate constants). Once again, we observe three equilibria: ($\overline{p_{open}} = 5.6 \times 10^{-4}$, $c_* = 0.11$), (0.25, 2.6), and (0.73, 7.3). Assuming the initial state of the channel is closed, Fig. 8B shows several Monte Carlo simulations that differ only by the initial $[Ca^{2+}]$ and demonstrate that the lower and upper equilibria of Fig. 8A are stable while the middle equilibrium is unstable. Here the domain time constant is quite slow (τ = 300 ms) and it takes several seconds for p_{open} and c_* to equilibrate. Figure 8C shows that although the relaxation to the equilibria is faster and the $[Ca^{2+}]$ fluctuations are larger, the graphical analysis is still essentially correct when the domain time constant is reduced to τ = 30 ms. Of course, τ can be reduced to the

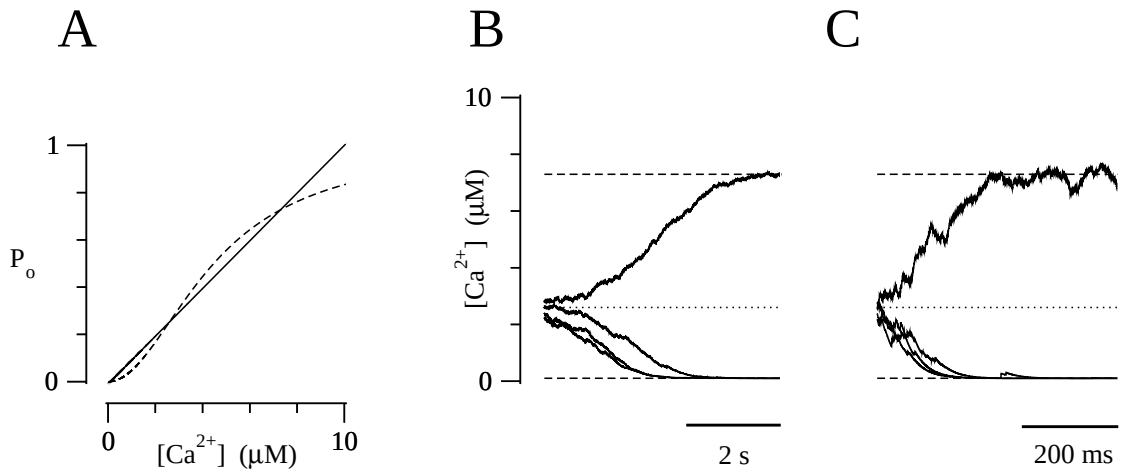

Figure 8: A: Linear dependence of c_* on $\overline{p_{open}}$ assumed by Eq. 21 (*solid line*) and $\overline{p_{open}}$ as a function of c_* for the two-state Ca^{2+}-activated channel (*dashed line*) given by Eq. 22 with $\eta = 2$, $k^+ = 200\ \mu M^{-1} ms^{-1}$ and $k^- = 4000\ ms^{-1}$. Intersections represent ($\overline{p_{open}}$,c_*) equilibria in the limit of a slow Ca^{2+} domain. B,C: $[Ca^{2+}]$ as a function of time during Monte Carlo simulations with initial value of 2.2, 2.4, 2.6 and 2.8 μM (*solid lines*) plotted with the unstable (*dotted line*) and stable (*dashed lines*) equilibria. In ms: $\tau = 300$ (B) and 30 (C).

point where the domain is no longer slow compared to channel dwell times and the graphical analysis does not apply.

3.3 Probability density formulation for the effect of residual Ca^{2+} on two-state channels

The analytical methods discussed in Section 3.2 give estimates of the effect of residual Ca^{2+} on p_{open} of two-state channels in the limit of a very fast or slow Ca^{2+} domain (small and large τ). An alternative and more sophisticated approach that allows analytic calculation of p_{open} without assuming an extreme value of τ begins with writing the probability density functions for the domain $[Ca^{2+}]$ jointly distributed with the state of the channel (Fox & Lu, 1994; Bertram & Sherman, 1998; Nykamp & Tranchina, 2000; Smith, 2002*a*),

$$\rho_i(c,t)dc \equiv \mathsf{P}\left\{c < [Ca^{2+}] < c + dc \text{ and } S(t) = \mathcal{S}_i\right\}.$$

Using Bayes' formula these probability densities can be related to the to the probability densities for domain $[Ca^{2+}]$ *conditioned* on the the state of the channel,

$$\mathsf{P}\left\{c < [Ca^{2+}] < c + dc \mid S(t) = \mathcal{S}_i\right\} = \frac{\mathsf{P}\left\{c < [Ca^{2+}] < c + dc \text{ and } S(t) = \mathcal{S}_i\right\}}{\mathsf{P}\left\{S(t) = \mathcal{S}_i\right\}}.$$

That is, if the probability density $\rho_i(c,t)$ is integrated over all possible Ca^{2+} concentrations, the probability of finding the channel in state i is obtained,

$$\pi_i \equiv \mathsf{P}\left\{S(t) = \mathcal{S}_i\right\} = \int_{c_\infty}^{c_{ss}} \rho_i(c,t)dc.$$

Although we are studying the the effect of residual Ca^{2+} on the gating of single channels, the probability density approach is appropriate. The densities $\rho_i(c,t)$ correspond to the probability of observing a given domain $[Ca^{2+}]$ (c) and channel state $(\mathcal{S}_i)$ at time t when sampling from a large number of identical Monte Carlo simulations such as Figs. 3 and 4.

Importantly, the time-dependent probability densities $\rho_i(c,t)$ can be related to one another, to the parameters of the single channel model, and to the assumed dynamics of the Ca^{2+} domain. To give a concrete example, consider the two-state Ca^{2+}-activated channel (Fig. 3) and write $\rho_C(c,t)$ and $\rho_O(c,t)$ as the joint probability density functions,

$$\begin{aligned}
\rho_C(c,t)dc &= \mathsf{P}\left\{c < [Ca^{2+}] < c + dc \text{ and } S(t) = C\right\} \\
\rho_O(c,t)dc &= \mathsf{P}\left\{c < [Ca^{2+}] < c + dc \text{ and } S(t) = O\right\}.
\end{aligned}$$

After a little thought, one can write a the following system of advection-reaction equations expressing a conservation law for these joint probability densities,

$$\frac{\partial \rho_C}{\partial t} = -\frac{\partial \phi_C}{\partial c} - k^+ c^\eta \rho_C + k^- \rho_O \tag{24}$$

$$\frac{\partial \rho_O}{\partial t} = -\frac{\partial \phi_O}{\partial c} + k^+ c^\eta \rho_C - k^- \rho_O \tag{25}$$

where ϕ_C and ϕ_O are probability fluxes given by

$$\phi_C(c,t) = j_C(c)\,\rho_C(c,t) \quad \text{where} \quad j_C(c) = -\frac{c - c_\infty}{\tau} \tag{26}$$

$$\phi_O(c,t) = j_O(c)\,\rho_O(c,t) \quad \text{where} \quad j_O(c) = \alpha_0 - \frac{c - c_\infty}{\tau} = -\frac{c - c_{ss}}{\tau}. \tag{27}$$

In these equations, the functions of $[Ca^{2+}]$ denoted by j_C and j_O correspond to the deterministic dynamics of the Ca^{2+} domain, i.e., the right hand side of Eq. 9—note that the source amplitude parameter α_0 is present in j_O but not j_C. Eqs. 24–27 represent a conservation law indicating that the time-evolution of probability density at any $[Ca^{2+}]$ can only change due to the impact of the distinct deterministic dynamics of $[Ca^{2+}]$ depending on channel

state (the advection terms) or the stochastic dynamics of the Ca^{2+} channel that occur with different kinetics depending on $[Ca^{2+}]$ (the reaction terms).

The boundary conditions for Eqs. 24–25 can be determined by considering the probability fluxes for the closed (ϕ_C) and open (ϕ_O) channel at the left (c_∞) and right (c_{ss}) boundary values for $[Ca^{2+}]$. Notice that j_C is negative in the biophysical range $c_\infty \leq c \leq c_{ss}$ and zero at c_∞ and, consequently, probability density associated with the closed state cannot advect across c_∞ from the right (i.e., from Ca^{2+} concentrations greater than c_∞). On the other hand, j_O is positive for $c_\infty \leq c \leq c_{ss}$ and *nonzero* at c_∞. To ensure that probability density associated with the open state does not advect across c_∞ from the left (i.e., from Ca^{2+} concentrations less than c_∞), we enforce $\phi_O(c_\infty, t) = 0$ (zero probability flux) which in turn implies $\rho_O(c_\infty, t) = 0$ (zero probability density). A similar argument for the upper boundary value (c_{ss}) leads to the condition $\rho_C(c_{ss}, t) = 0$ to ensure $\phi_C(c_{ss}, t) = 0$. Thus, the boundary conditions that we associate with Eqs. 24–25 are,

$$\rho_C(c_{ss}, t) = 0 \tag{28}$$

$$\rho_O(c_\infty, t) = 0. \tag{29}$$

Notice that for both Eqs. 24 and 25, the joint probability density (ρ_i, $i \in \{C, O\}$) is constrained to be zero at the *one* boundary (either c_∞ or c_{ss}) where the advection rate (j_i) is nonzero; consequently, each equation has one associated boundary condition, as required.

— ◇ ◇ ◇ —

While Eqs. 24–27 can be solved numerically (see last paragraph of Appendix C), here we focus on stationary (time-independent) solutions that can be obtained analytically. Setting the time derivatives to zero, we find that for the Ca^{2+}-activated channel,

$$0 = -\frac{d}{dc}\left[j_C \rho_C\right] - k^+ c^\eta \rho_C + k^- \rho_O \tag{30}$$

$$0 = -\frac{d}{dc}\left[j_O \rho_O\right] + k^+ c^\eta \rho_C - k^+ \rho_O \tag{31}$$

where $\rho_C(c)$ and $\rho_O(c)$ are functions of $[Ca^{2+}]$ but not time. Notice that if a stationary solution (ρ_C, ρ_O) of Eqs. 30–31 is found, then $(\hat{\rho}\rho_C, \hat{\rho}\rho_O)$ is also a solution where $\hat{\rho}$ is an arbitrary constant. This constant is constrained by conservation of probability, that is,

$$\int_{c_\infty}^{c_{ss}} \left[\rho_C(c) + \rho_O(c)\right] dc = 1. \tag{32}$$

Given an appropriately scaled set of time-independent solutions, the equilibrium open probability is found by integrating the joint probability density for the open state over all Ca^{2+}

concentrations,

$$p_{open} = \int_{c_\infty}^{c_{ss}} \rho_O(c) dc. \tag{33}$$

As mentioned above, this expression for p_{open} corresponds to the equilibrium open probability that would be observed in a long Monte Carlo simulation such as those presented in Section 3.1. We can think of $\rho_C(c)$, $\rho_O(c)$, and the final answer, p_{open}, as being parameterized by the domain time constant (τ) as both j_C and j_O contain this parameter.

— ◇ ◇ ◇ —

The first step in solving Eqs. 30–31 is to sum them and conclude that at steady state the total probability flux $\phi_T \equiv \phi_C + \phi_O = j_C\rho_C + j_O\rho_O$ satisfies

$$0 = -\frac{d}{dc}\left[j_C\rho_C + j_O\rho_O\right].$$

This implies that ϕ_T is constant (not a function of c) and furthermore this constant must be zero to satisfy the boundary conditions (Eqs. 28 and 29). Thus, we can write

$$j_C\rho_C + j_O\rho_O = -\frac{c - c_\infty}{\tau}\rho_C - \frac{c - c_{ss}}{\tau}\rho_O = 0$$

where we have used Eqs. 26 and 27. Because $\phi_T = 0$ the probability fluxes $\phi_C(c) < 0$ and $\phi_O(c) > 0$ are equal and opposite and we can express ρ_C as a function of ρ_O,

$$\rho_C = \frac{c_{ss} - c}{c - c_\infty}\rho_O. \tag{34}$$

Using this expression we eliminate Eq. 30 to obtain,

$$0 = -\frac{d}{dc}\left[-\frac{c - c_{ss}}{\tau}\rho_O\right] + k^+c^\eta\frac{c_{ss} - c}{c - c_\infty}\rho_O - k^-\rho_O$$

which after differentiating and rearranging gives the following linear ordinary differential equation for ρ_O,

$$\frac{d\rho_O}{dc} = \left(\frac{1 - \tau^-}{c_{ss} - c} + \frac{\tau^+c^\eta}{c - c_\infty}\right)\rho_O \tag{35}$$

where $\tau^+ \equiv k^+\tau$ and $\tau^- \equiv k^+\tau$. Assuming for the moment that $\eta = 1$, we can separate variables and integrate to find

$$\ln\rho_O - \ln\bar{\rho}_O = \int_{\bar{c}}^{c}\left(\frac{\tau^- - 1}{c - c_{ss}} + \frac{\tau^+c}{c - c_\infty}\right)dc \tag{36}$$

$$= \left(\tau^- - 1\right)\ln\left(\frac{c_{ss} - c}{c_{ss} - \bar{c}}\right) + \tau^+\left(c - \bar{c}\right) + \tau^+c_\infty\ln\left(\frac{c - c_\infty}{\bar{c} - c_\infty}\right) \tag{37}$$

where $\bar{c}$ is some point on the interior ($c_\infty < \bar{c} < c_{ss}$), $\rho_O(\bar{c}) = \bar{\rho}_O$, and we have eliminated absolute value signs in the logarithms using $c \le c_{ss}$ and $c_\infty \le c$. Exponentiating Eq. 37 and using Eq. 34 we find,

$$\rho_C = \hat{\rho} e^{\tau^+ c} (c_{ss} - c)^{\tau^-} (c - c_\infty)^{\tau^+ c_\infty - 1} \tag{38}$$

$$\rho_O = \hat{\rho} e^{\tau^+ c} (c_{ss} - c)^{\tau^- - 1} (c - c_\infty)^{\tau^+ c_\infty} \tag{39}$$

where $\hat{\rho}$ is a constant chosen to satisfy conservation of probability (Eq. 32). Finally, we use Eq. 33 and a similar expression for p_{closed} to arrive at an expression for the equilibrium probabilities of the two-state Ca^{2+}-activated channel,

$$p_{open} = \hat{\rho} \int_{c_\infty}^{c_{ss}} e^{\tau^+ c} (c_{ss} - c)^{\tau^- - 1} (c - c_\infty)^{\tau^+ c_\infty} \, dc. \tag{40}$$

Note that the constant $\hat{\rho}$ does not have to be found when both Eq. 38 and 39 are integrated because

$$p_{open} = \frac{1}{1+\xi} \qquad \text{where} \qquad \xi = \frac{p_{closed}}{p_{open}} = \frac{\int_{c_\infty}^{c_{ss}} e^{\tau^+ c} (c_{ss} - c)^{\tau^-} (c - c_\infty)^{\tau^+ c_\infty - 1} \, dc}{\int_{c_\infty}^{c_{ss}} e^{\tau^+ c} (c_{ss} - c)^{\tau^- - 1} (c - c_\infty)^{\tau^+ c_\infty} \, dc}$$

and ξ does not depend on $\hat{\rho}$. Appendix B shows the derivation of the steady-state joint probability densities ρ_C and ρ_C for cooperativity of Ca^{2+} binding η greater than 1.

— ◇ ◇ ◇ —

Figure 9 plots these analytical expressions for the stationary joint probability densities ρ_C (Eq. 39, *top panels*) and ρ_O (Eq. 38, *bottom panels*). In Fig. 9A the domain is comparatively fast (τ small) so the probability density accumulates near c_∞ when the channel is closed and c_{ss} when the channel is open. Consistent with Eq. 38, $\rho_C \to \infty$ as $c \to c_\infty$ from above because $\tau^+ c_\infty < 1$ in Fig. 9A, i.e., there is a negative exponent in the $(c - c_\infty)$ term of ρ_C. Because $\tau^- < 1$, ρ_O also diverges as $c \to c_{ss}$ from below. Although ρ_C and ρ_O diverge, they remain integrable as probability densities must. Figure 9B shows the probability densities for a slower domain; here ρ_C has shifted toward higher $[Ca^{2+}]$. In Fig. 9C the Ca^{2+} domain is quite slow (large τ) and the range of Ca^{2+} concentrations likely to be observed is approximately the same regardless of whether the channel is open or closed. All of these observations are consistent with the Monte Carlo simulations presented in Fig. 3. Indeed, Figure 9A–C and Fig. 3A–C use the same values of τ and can be directly compared. Also notice that these plots satisfy the boundary conditions (Eqs. 28–29).

— ◇ ◇ ◇ —

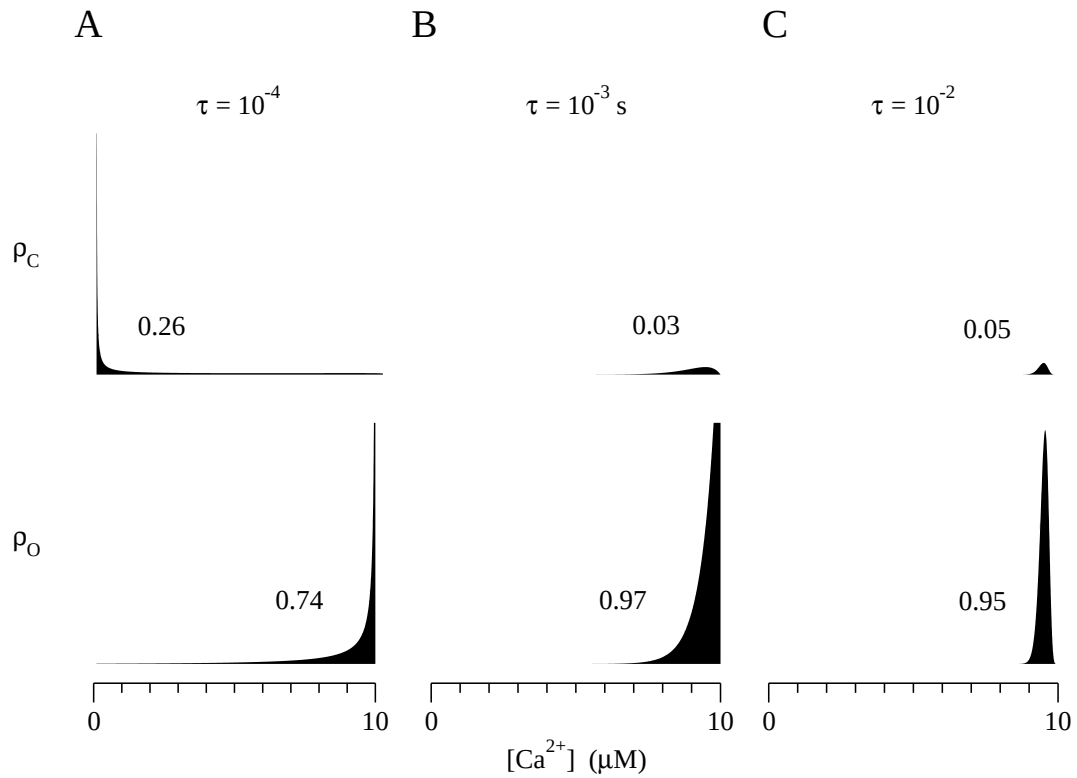

Figure 9: The joint probability densities ρ_C (*top panels*) and ρ_O (*bottom panels*) given by Eqs. 38 and 39 for the two-state Ca^{2+}-activated channel are plotted for three different Ca^{2+} domain time constants: $\tau = 10^{-4}$ (A), 10^{-3} (B), and 10^{-2} s (C). Scaling of y-axis changes in A–C for clarity, but is identical for each (ρ_C,ρ_O) pair. The numerical values near each density gives the integrated area corresponding to p_{closed} and p_{open}. Probability densities that diverge at c_∞ or c_{ss} are clipped.

Figure 10 is similar to Fig. 9 except that the stationary joint probability densities ρ_C and ρ_O are plotted for the Ca^{2+}-inactivated channel. In this case ρ_C and ρ_O solve,

$$0 = -\frac{d}{dc}\left[j_O\rho_O\right] - k^+c^\eta\rho_O + k^-\rho_C$$
$$0 = -\frac{d}{dc}\left[j_C\rho_C\right] + k^+c^\eta\rho_O - k^-\rho_C$$

and repeating the analytical work presented above,

$$\rho_C = \hat{\rho}e^{\tau^+c}\left(c_{ss}-c\right)^{\tau^+c_{ss}}\left(c-c_\infty\right)^{\tau^--1} \tag{41}$$
$$\rho_O = \hat{\rho}e^{\tau^+c}\left(c_{ss}-c\right)^{\tau^+c_{ss}-1}\left(c-c_\infty\right)^{\tau^-}. \tag{42}$$

Thus, we find that for the Ca^{2+}-inactivated channel,

$$p_{open} = \hat{\rho}\int_{c_\infty}^{c_{ss}} e^{\tau^+c}\left(c_{ss}-c\right)^{\tau^+c_{ss}-1}\left(c-c_\infty\right)^{\tau^-}dc. \tag{43}$$

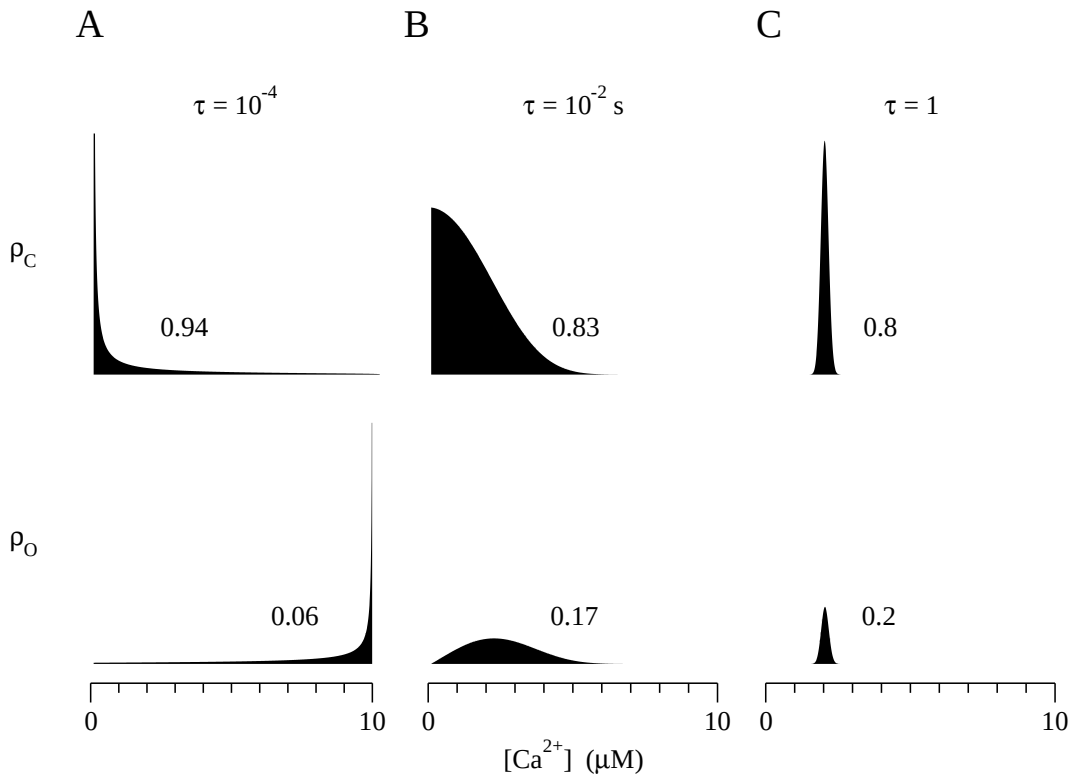

Figure 10: The joint probability densities ρ_C (*top panels*) and ρ_O (*bottom panels*) given by Eqs. 41 and 41 for the two-state Ca^{2+}-inactivated channel are plotted for three different Ca^{2+} domain time constants: $\tau = 10^{-4}$ (A), 10^{-2} (B), and 1 s (C). Scaling of y-axis changes in A–C for clarity. See legend to Fig. 9.

As expected, there are similarities between these expressions and Eqs. 38–40. In particular, Fig. 10 shows that the stationary joint probability densities ρ_C and ρ_O go through a similar transition as the domain time constant (τ) increases. Though p_{open} is significantly different in the two cases, for small τ both ρ_C and ρ_O diverge and the probability density accumulates near c_∞ and c_{ss}, respectively (cf. Fig. 9A), while for large τ (Fig. 10C) the range of Ca^{2+} concentrations spanned by ρ_C and ρ_O are similar.

— ◇ ◇ ◇ —

The final results of the analytical calculations presented above are the equilibrium open probabilities for the Ca^{2+}-activated and Ca^{2+}-inactivated channels given by Eq. 40 and Eq. 43, respectively. Numerically (or even visually) integrating the joint probability densities of comparatively slow domains (e.g., Fig. 9C) yields integrated areas of ρ_C and ρ_O that are consistent with p_{open} from Monte Carlo simulations (Fig. 3C) and analytical results (Fig. 5).

However, for fast domains (small τ) the divergence of the probability densities near the boundaries makes such comparisons difficult. In particular, when $\rho_O \to \infty$ as $c \to c_{ss}$ from below it is difficult to accurately calculate p_{open} by numerically evaluating the integrals in Eq. 40 and Eq. 43.

Indeed, some care is required even when plotting the closed form solutions for ρ_C and ρ_O (Figs. 9 and 10). Because the exponential factor $e^{\tau^+ c}$ in Eqs. 38 and 39 can move through a tremendous range as c increases from c_∞ to c_{ss}, we produce Figs. 9 and 10 by calculating $\ln \rho_C$ and $\ln \rho_O$ and subsequently shifting these quantities (corresponding to changing the factor $\hat{\rho}$) so that the interesting regions of the curves can be exponentiated without numerical overflow.

Because of such concerns, it is helpful to recognize that the integral expressions for p_{open} for Ca^{2+}-activated (Eq. 40) and Ca^{2+}-inactivated (Eq. 43) channels correspond to a well-known special function. Writing $c_d = c_{ss} - c_\infty$ and $x = (c - c_\infty)/c_d$ and changing variables, Eq. 40 becomes

$$p_{open} = \hat{\rho} e^{\tau^+ c_\infty} c_d^{\tau^- + \tau^+ c_\infty} \int_0^1 e^{\tau^+ c_d x} (1-x)^{\tau^- - 1} x^{\tau^+ c_\infty} dx.$$

The integral in this expression is of the form

$$\int_0^1 e^{zt} t^{a-1} (1-t)^{b-a-1} dt = \frac{\Gamma(b-a)\Gamma(a)}{\Gamma(b)} M(a,b,z) \tag{44}$$

where $M(a,b,z)$ is a confluent hypergeometric function known as Kummer's function that can be evaluated with the series

$$M(a,b,z) = 1 + \frac{az}{b} + \frac{(a)_2 z^2}{(b)_2 2!} + \cdots + \frac{(a)_n z^n}{(b)_n n!} + \cdots$$

with $(a)_n = a(a+1)\cdots(a+n-1)$ and similarly for $(b)_n$. Thus, for the two-state channel activated by Ca^{2+}, the equilibrium open probability is given by

$$p_{open} = \hat{\rho} e^{\tau^+ c_\infty} c_d^{\tau^- + \tau^+ c_\infty} \frac{\Gamma(\tau^-)\Gamma(\tau^+ c_\infty + 1)}{\Gamma(\tau^- + \tau^+ c_\infty + 1)} M\left(\tau^+ c_\infty + 1, \tau^- + \tau^+ c_\infty + 1, \tau^+ c_d\right),$$

while for the two-state Ca^{2+}-inactivated channel,

$$p_{open} = \hat{\rho} e^{\tau^- c_\infty} c_d^{\tau^- + \tau^+ c_{ss}} \frac{\Gamma(\tau^+ c_{ss})\Gamma(\tau^- + 1)}{\Gamma(\tau^+ c_{ss} + \tau^- + 1)} M\left(\tau^- + 1, \tau^+ c_{ss} + \tau^- + 1, \tau^+ c_d\right).$$

These analytical solutions shown as the *solid* and *dotted lines* in Fig. 5 agree with Monte Carlo simulations (*filled circles* and *open squares*) for a range of domain time constants (τ).

3.4 Numerical estimates of the effect of residual Ca^{2+} on arbitrarily complex channel models

Our interest in the effect of residual Ca^{2+} on channel gating certainly extends beyond simple two-state models. For example, the probability density approach described in Section 3.3 can be generalized to arbitrarily complex single channel models (see Section 3.7 and Appendix C). This section presents a numerical method for calculating the effect of residual Ca^{2+} on arbitrarily complex single channel models in the limit of a very fast or very slow Ca^{2+} domain (cf. Section 3.2).

Given an M-state single channel model of a Ca^{2+}-regulated Ca^{2+} channel (Eq. 5), the small τ limit is calculated simply by associating the appropriate $[Ca^{2+}]$ with closed (c_∞) and open (c_{ss}) states. Writing $\underline{Q}$ for the modified generator matrix,

$$\underline{Q} = K_- + \mathrm{diag}\left\{c_\infty \boldsymbol{u}_C + c_{ss}\boldsymbol{u}_O\right\}^\eta K_+, \tag{45}$$

the equilibrium open probability in the small τ limit ($\underline{p_{open}}$) can be found using the probability distribution satisfying global balance, that is,

$$\underline{p_{open}} = \underline{\boldsymbol{\pi}}\boldsymbol{u}_O \quad \text{where} \quad \underline{\boldsymbol{\pi}}\underline{Q} = \mathbf{0} \quad \text{and} \quad \underline{\boldsymbol{\pi}}\boldsymbol{e} = 1. \tag{46}$$

When the Ca^{2+} domain forms and collapses slowly compared to channel gating (large τ limit), then the Ca^{2+} binding site experiences essentially the same $[Ca^{2+}]$ (c_*) regardless of channel state. In this large τ limit, the modified generator matrix $\overline{Q}$ is given by

$$\overline{Q} = K_- + c_*^\eta K_+ \qquad \text{where} \qquad c_* = \overline{p_{open}}c_{ss} + c_\infty\left(1 - \overline{p_{open}}\right). \tag{47}$$

To find c_* and p_{open}, we simultaneously solve Eq. 47 and

$$\overline{p_{open}} = \overline{\boldsymbol{\pi}}\boldsymbol{u}_O \quad \text{where} \quad \overline{\boldsymbol{\pi}}\overline{Q} = \mathbf{0} \quad \text{and} \quad \overline{\boldsymbol{\pi}}\boldsymbol{e} = 1. \tag{48}$$

There will be at least one solution pair (p_{open}, c_*), but as seen in Sections 3.1 and 3.2 multiple solutions are certainly possible as well.

3.5 The effect of residual Ca^{2+} on the De Young-Keizer IP_3R model

In this section we analyze the effect of residual Ca^{2+} on a realistic Ca^{2+} channel model, the De Young-Keizer IP_3R, using both Monte Carlo simulation and the method of Section 3.4. As described in some detail in Section 2.2, the De Young-Keizer model views the IP_3R as a

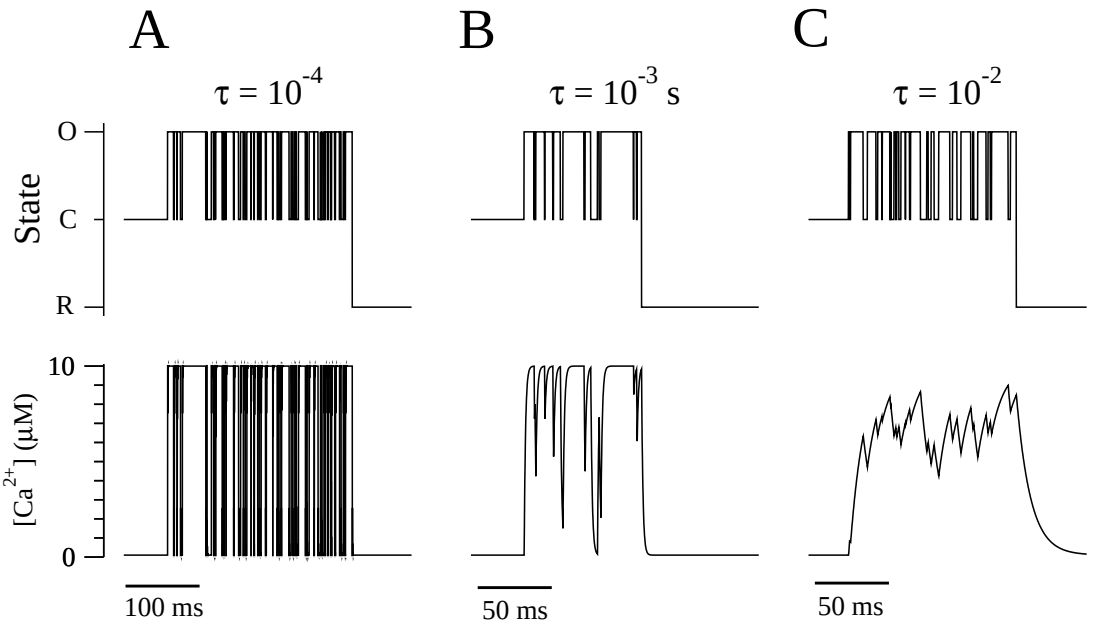

Figure 11: Monte Carlo simulations of the De Young-Keizer IP_3R model with a time-dependent Ca^{2+} domain modeled by Eq. 9 using three comparatively small values of domain time constant (τ). Sojourns in open (O), closed (C), and refractory (R) states are plotted as a function of time. Parameters as Table 1.

collection of identical subunits, each of which has one binding site for IP_3 and two binding sites for Ca^{2+} (De Young & Keizer, 1992). We assume four subunits leading to a generator matrix with 4096 states, 330 of which are distinguishable.

Figure 11 shows Monte Carlo simulations of the De Young-Keizer IP_3R model stochastically gating in the presence of a time-dependent Ca^{2+} domain (Eq. 9). In this figure state O is, of course, the one open state: (6,6,6,6). When one or more of the four subunits has inactivating Ca^{2+} bound—S_1, S_3, S_5, and S_7 in Fig. 2—the channel is considered refractory (R). All other states are simply closed (C). The values of τ used in Figure 11 are all small compared to the time scale of Ca^{2+} inactivation, but they are fast (A), intermediate (B) or slow (C) with respect to Ca^{2+} activation. Figure 11A shows the De Young-Keizer IP_3R model gating with a fast domain—here both closed and refractory states usually experience the background $[Ca^{2+}]$ (c_∞). In Fig 11C the domain is slower and while the refractory state experiences c_∞, the fast transitions between open and closed states cause the closed states to often experience elevated $[Ca^{2+}]$. As the domain time constant increases in Fig. 11A–C the range of Ca^{2+} concentrations observed during bursts of $C \leftrightharpoons O$ transitions becomes restricted, that is, the domain $[Ca^{2+}]$ experienced by the closed state increases while the

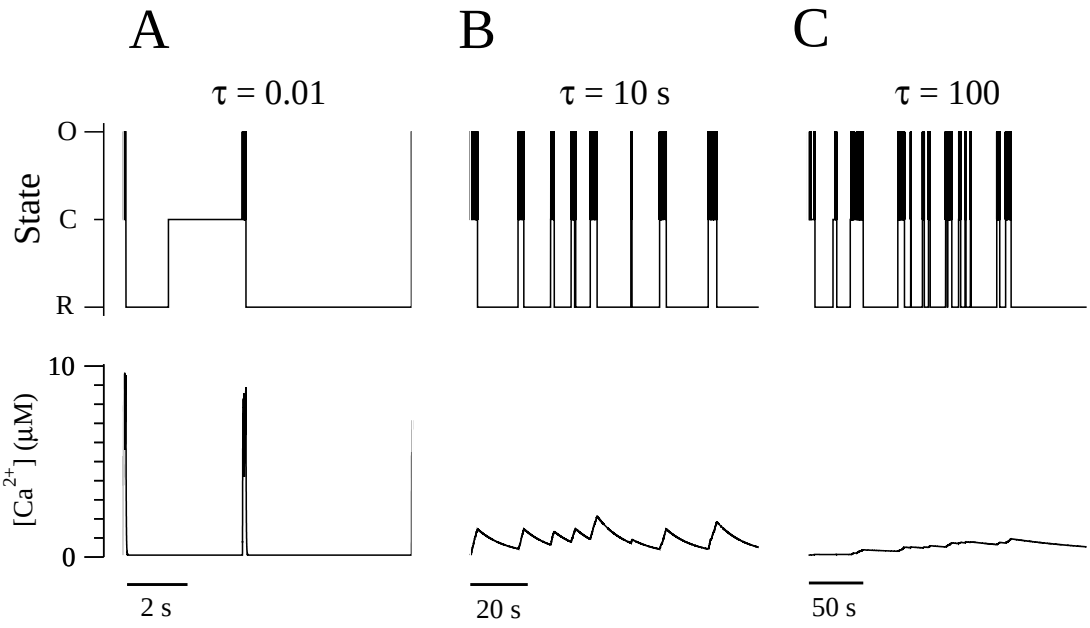

Figure 12: Monte Carlo simulations of the De Young-Keizer IP_3R model using three comparatively large values of domain time constant (τ). See legend to Fig. 11.

domain [Ca^{2+}] experienced by the open state decreases (cf. Figs. 9 and 10).

Figure 12A shows the same results as Fig 11C rescaled to show several long-lived closed (i.e., refractory) states. The domain time constant of $\tau = 0.01$ s is slow compared to Ca^{2+}-activation, but fast compared to Ca^{2+}-inactivation, and on this time scale it is clear that the refractory states (R) experiences the background [Ca^{2+}] (c_∞). When τ is comparable to the time scale of Ca^{2+}-inactivation in Figure 12B (seconds rather than milliseconds), the open, closed, and refractory states all experience elevated [Ca^{2+}]. When the domain is slow compared to Ca^{2+}-inactivation (Fig 12C), fluctuations in [Ca^{2+}] decrease still further and open, closed, and refractory states all experience similar domain [Ca^{2+}].

Figure 13A summarizes the observed open probability of the De Young-Keizer IP_3R model calculated by Monte Carlo simulation for a range of domain time constants (*filled circles*). In these simulations the source amplitude of the channel α_0 is adjusted so that regardless of τ the maximum [Ca^{2+}] experienced by the channel is $c_{ss} = 10$ μM. Note that although the equilibrium open probability of the De Young-Keizer IP_3R model is a bell-shaped function of [Ca^{2+}] (De Young & Keizer, 1992), the observed p_{open} is a monotonically increasing function of the domain time constant when c_{ss} is fixed. Although this may be counter-intuitive, it is consistent with the two-state model results where both Ca^{2+}-activation and Ca^{2+}-inactivation lead to p_{open} that was an increasing function of τ (recall *filled circles*

and *solid lines* of Fig. 5).

Figure 13B shows the case when α_0 is fixed and increasing the domain time constant (τ) results in increased domain size (c_{ss}). Here, p_{open} of the De Young-Keizer model *decreases* as a function of τ, a result similar to the two-state Ca^{2+}-inactivated channel when α_0 is fixed (*open squares* and *dotted lines* of Fig. 5B) and different from the Ca^{2+}-activated channel model (*open squares* and *dotted lines* of Fig. 5A). While the De Young-Keizer-like IP_3R model responds to residual Ca^{2+} with a steady state open probability that is a monotonic function of the domain time constant, other channel models that include both Ca^{2+}-activation and Ca^{2+}-inactivation show more complex behavior (see below).

The Monte Carlo simulation results using the De Young-Keizer model are in agreement with the small and large τ limits directly calculated from the 330 state generator using Eqs. 45–46 (fast domain, *dotted line*) and Eqs. 47–48 (slow domain, *solid line*). This verifies both calculations and shows that for realistic models of intracellular Ca^{2+} channels the methods presented in Section 3.4 are applicable. Interestingly, analytical estimates of p_{open} of the De Young-Keizer model in the small and large τ limits can be obtained using the separation of time scales between activation and inactivation (see Appendix D). In three of four cases these results are not distinguishable from the more rigorous numerical estimates given by Eqs. 45–48. The *dot-dashed line* of Fig. 13A show the one case that is distinguishable from the numerical estimate, but even here the analytical approximation works well. However, the numerical estimates of the small and large τ limits give no indication of the value of τ leading to half-maximal p_{open} or other quantitative information when τ is in this intermediate range. Monte Carlo simulation—or, alternatively, the more sophisticated techniques discussed in Section 3.7 and Appendix C—are required to observe the effects of residual Ca^{2+} at intermediate values of τ.

3.6 Modeling the effect of residual Ca^{2+} using reaction-diffusion equations

While the analysis of the effect of residual Ca^{2+} on the stochastic gating of Ca^{2+} channels presented above has focused on the case of a dynamic Ca^{2+} domain formed in a restricted cytoplasmic compartment, the approach can also be applied to the case of a homogeneous isotropic cytosol where the Ca^{2+} domain is modeled using the equations for the buffered diffusion of intracellular Ca^{2+} (see Section 2.3). We focus on the effect of residual Ca^{2+} in the presence of a single high concentration Ca^{2+} buffer where cytoplasmic Ca^{2+} concentration $c(r,t)$ is a function of space and time solving the cable equation (Eq. 14). The Ca^{2+} binding site of the channel is located a short distance ($r_0 = 0.02$ μm) from the channel pore and

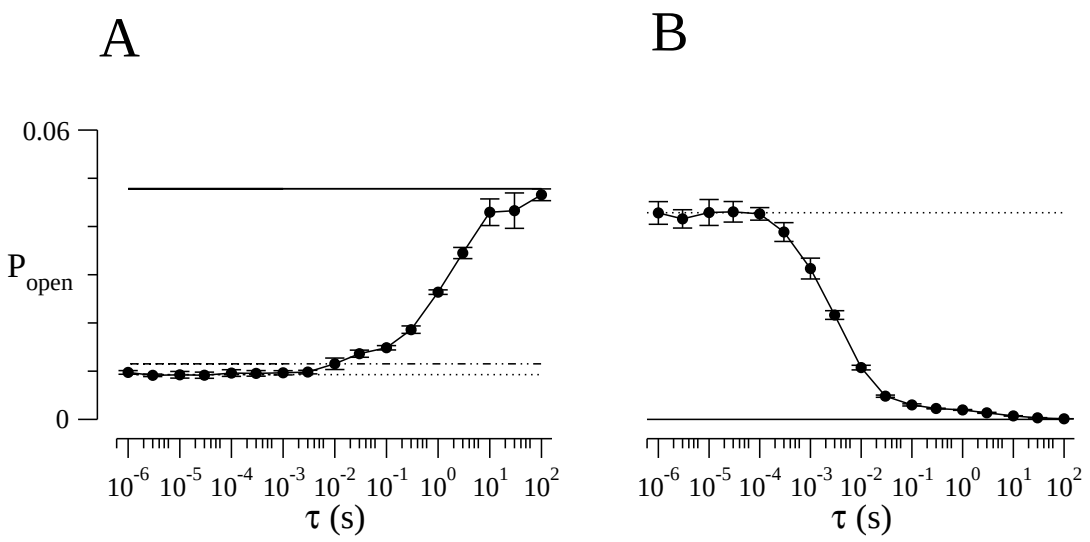

Figure 13: Summary of the effect of the domain time constant (τ) on the observed open probability (p_{open}) of the the De Young-Keizer IP_3R model. Monte Carlo results (*filled circles*) agree with numerical estimates of p_{open} for fast or slow domains (*dotted* and *solid lines*, respectively). A: The source amplitude (α_0) of the channel is adjusted so that regardless of τ the maximum $[Ca^{2+}]$ experienced by the channel is $c_{ss} = 10$ μM. B: The source amplitude (α_0) is fixed at 990 μM/s and increasing the domain time constant (τ) results in increased domain size (c_{ss}). Parameters as Fig. 11.

the local $[Ca^{2+}]$ that influences channel gating is $c(r_0, t)$. The buffer length (λ) and time (θ) constants are varied over a considerable range.

As in many of the simulations presented above, we adjust the source amplitude σ_0 to maintain a fixed maximum $[Ca^{2+}]$ at the binding site of $c_{ss} = 10$ μM. Inverting Eq. 16, this implies that for any choice of λ and θ,

$$\sigma_0 = 2\pi D_c r_0 \left(c_{ss} - c_\infty\right) e^{r_0/\lambda} \qquad \text{where} \qquad D_c = \lambda^2/\theta. \tag{49}$$

In other simulations, the source amplitude will be fixed and the domain $[Ca^{2+}]$ will increase or decrease as θ and λ are varied. The source amplitude in this case is $\sigma_0 = 341$ μmoles/sec, corresponding to a 0.066 pA channel when the buffer parameters mentioned in Section 2.3 for millimolar EGTA are used ($[B]_T = 1000$ μM, $k_{on}^{buf} = 1.5$ $\mu M^{-1}s^{-1}$, $k_{off}^{buf} = 0.3$ s^{-1}, $K^{buff} = 0.2$ μM). This implies buffer length and time constants of $\lambda = \sqrt{D_c/k_{on}^{buf}[B]_\infty} = 0.5$ μm and $\theta = \lambda^2/D_c = 1$ ms—calculated using $c_\infty = 0.1$ μM, $D_c = 250$ $\mu m^2/s$, and $[B]_\infty = K^{buff}[B]_T/\left(K^{buff} + c_\infty\right) = 667$ μM—but these representative values are of little significance

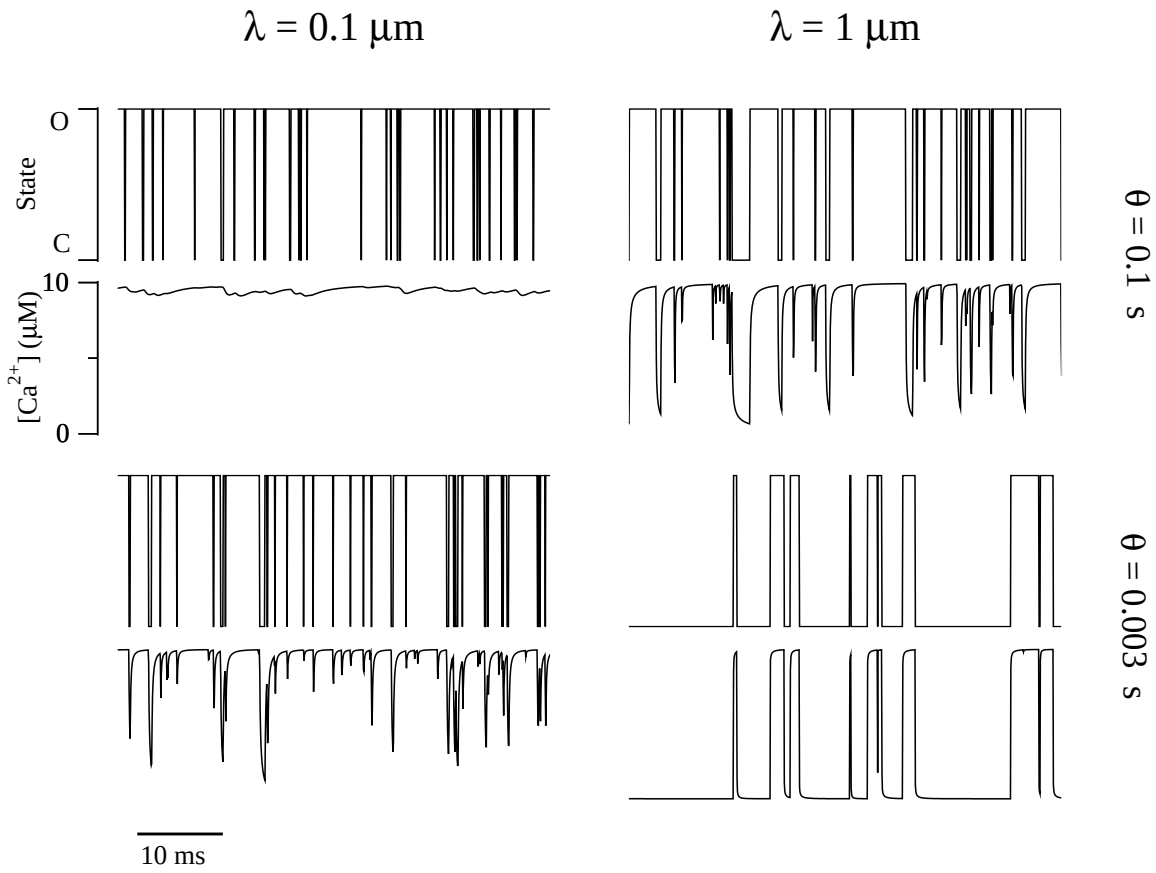

Figure 14: Monte Carlo simulations of a two-state Ca^{2+}-activated channel gating in the presence of a Ca^{2+} domain formed in a homogeneous isotropic cytosol (Eq. 14). The time constant (θ = 0.003, 0.1 s) and length constant (λ = 0.1, 1 μm) of a single high concentration Ca^{2+} buffer are both varied. Parameters as Fig. 3 with r_0 = 0.021 μm and σ_0 given by Eq. 49 so that the maximum domain $[Ca^{2+}]$ at r_0 is 10 μM corresponding to a range of diffusion coefficients and source amplitudes, e.g., when θ = 0.003 s and λ = 1 μm D_c = 333 μm^2/s and i_{Ca} = 0.086 pA.

because in this section λ and θ are varied over a wide range (see below).

Also note that with initial conditions $c(r, t = 0) = c_\infty$, the solution of the radial cable equation (Eq. 14) with a constant source σ_0 is given by

$$c(r,t) = c_\infty + \frac{\sigma_0}{8\pi D r}\left[e^{-\zeta}\mathrm{erfc}\left(\frac{\zeta}{2\sqrt{T}} - \sqrt{T}\right) + e^{\zeta}\mathrm{erfc}\left(\frac{\zeta}{2\sqrt{T}} + \sqrt{T}\right)\right] \tag{50}$$

where $\zeta = r/\lambda$ and $T = t/\theta$. From this expression, we see that the parameter θ is not an *exponential* time constant and is thus distinct from the domain time constant τ that occurs in the ordinary differential equations for the dynamics of $[Ca^{2+}]$ in a restricted cytosolic compartment (Eq. 9).

Figure 14 presents Monte Carlo simulations of a two-state Ca^{2+}-activated channel gating in the presence of a Ca^{2+} domain formed in a homogeneous isotropic cytosol (Eq. 14) with

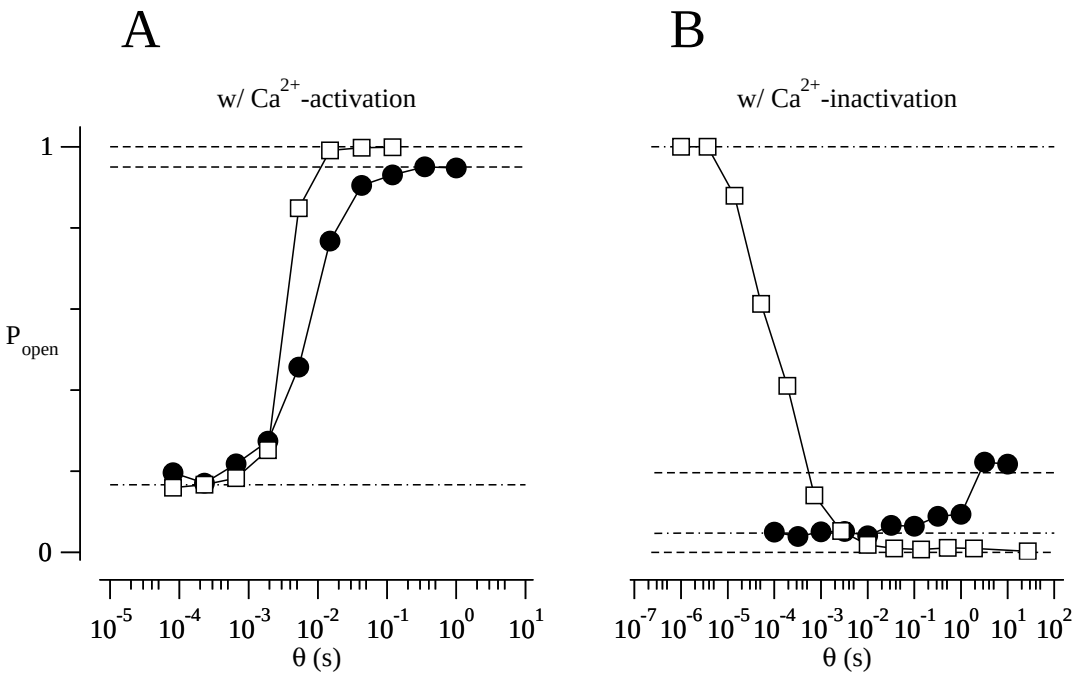

Figure 15: Summary of the effect of the Ca^{2+} domain time constant (θ) on the observed open probability (p_{open}) of the two-state Ca^{2+}-activated (A) and Ca^{2+}-inactivated (B) channels gating in a homogeneous isotropic cytosol (Eq. 14) using fixed c_{ss} (*filled circles*) or fixed source amplitude (*open squares*). Analytical estimates described in Section 3.2 give p_{open} in the limit of small (*dot-dashed*) and large (*dashed lines*) λ agree with Monte Carlo simulations (*filled circles* and *open squares*). The buffer length constant $\lambda = 0.5$ μm while $D_c = \lambda^2/\theta$ varies. Other parameters as Fig. 14.

c_{ss} fixed at 10 μM (Eq. 49). Consistent with Eq. 50 these calculations show that domain $[Ca^{2+}]$ often exhibits a fast initial increase (or decrease) followed by a slower relaxation. Comparing two simulations in the same column that use identical buffer length constants (λ) but different buffer time constants (θ), we see that larger values of θ results in smaller fluctuations in the local $[Ca^{2+}]$. This is similar to what was described above as a slow domain, except that here the formation and collapse of the Ca^{2+} domain is not exponential in nature (cf. Figs. 3 and 4). Comparing two simulations in the same row that use identical buffer time constants (θ) shows that small λ also results in smaller fluctuations. Thus, in the case of a homogeneous isotropic cytosol in the excess buffer limit, the domain appears 'slow' when the buffer time constant (θ) is large but also when the free Ca^{2+} diffusion coefficient ($D_c = \lambda^2/\theta$) is small.

Figure 15A and B summarize Monte Carlo simulations such as Fig. 14 using the two-state

channel model that is either activated (A) or inactivated (B) by Ca^{2+}. The simulations are once again performed with the maximum domain $[Ca^{2+}]$ or the source amplitude fixed (*filled circles* and *open squares*, respectively). In these calculations the buffer length constant is fixed at $\lambda = 0.5$ μm and thus the free Ca^{2+} diffusion coefficient ($D_c = \lambda^2/\theta$) is inversely proportional to the buffer time constant (θ) as it is varied. Because the parameter θ in the homogeneous isotropic cytosol is analogous to the exponential time constant τ that appears in the restricted cytosolic domain, there is a marked similarity between Fig. 15 and Fig. 5. A slow domain (large θ) increases p_{open} of the Ca^{2+}-activated channel regardless of whether c_{ss} or α_0 is fixed (*filled circles*). In the case of the Ca^{2+}-inactivated channel, p_{open} either increases or decreases depending on whether c_{ss} or α_0 is fixed (*open squares*).

3.7 The effect of residual Ca^{2+} may depend on multiple time scales of channel kinetics

In the simulations of the effect of residual Ca^{2+} on the stochastic gating of the De Young-Keizer IP_3R model using restricted cytosolic compartment (Section 3.5), we found that channel open probability depended on the relationship of the domain time constant to the time scales of both activation and inactivation. To explore these dynamics further, we extended the probability density method for calculating p_{open} at intermediate values of τ to channel models that have more than two states (assuming a restricted cytosolic compartment as in Section 3.3). The new approach involves numerically integrating time-dependent advection-reaction equations that are a generalization of Eqs. 24–27 for arbitrarily complex channel models (see Appendix C). This section uses this method, traditional Monte Carlo simulation, and a minimal model that includes both Ca^{2+} activation and inactivation to explore how the existence of two distinct time scales for channel kinetics may influence the effect of residual Ca^{2+} on channel open probability.

The channel model we consider includes two binding sites for Ca^{2+}—one for Ca^{2+}-activation and one for Ca^{2+}-inactivation—with no assumption of sequential binding. That

is, the transition-state diagram includes the following four states,

$$\begin{array}{ccccc} & & k_a^+ c & & \\ \text{(closed)} \quad C_1 & & \rightleftharpoons & & O \quad \text{(open)} \\ & & k_a^- & & \\ k_d^+ c \;\downarrow\uparrow\; k_d^- & & & & k_b^- \;\uparrow\downarrow\; k_b^+ c \\ & & k_c^- & & \\ \text{(closed)} \quad C_3 & & \leftrightharpoons & & C_2 \quad \text{(closed)} \\ & & k_c^+ c & & \end{array} \tag{51}$$

where the left-to-right transitions represent Ca^{2+}-activation and top-to-bottom transitions represent Ca^{2+}-inactivation. Because this model includes a cycle we are careful to choose parameters that satisfy the thermodynamic constraint $K_c K_d = K_a K_b$ (Hill, 1977) where the $K_i = k_i^-/k_i^+$ for $i \in \{a, b, c, d\}$ are dissociation constants. That is, there are eight rate constants in Eq. 51, but only seven are free parameters because $k_d^- = k_d^+ K_a K_b / K_c$. Enumerating states $\mathcal{M} = (C_1, O, C_2, C_3)$, the infinitesimal generator of this four-state model can be put in the form of Eq. 5,

$$Q = \begin{pmatrix} \diamond & 0 & 0 & 0 \\ k_a^- & \diamond & 0 & 0 \\ 0 & k_b^- & \diamond & k_c^- \\ k_d^- & 0 & 0 & \diamond \end{pmatrix} + c \begin{pmatrix} \diamond & k_a^+ & 0 & k_d^+ \\ 0 & \diamond & k_b^+ & 0 \\ 0 & 0 & \diamond & 0 \\ 0 & 0 & k_c^+ & \diamond \end{pmatrix} \tag{52}$$

where the cooperativity of Ca^{2+} binding is $\eta = 1$. Column vectors indicating closed and open states are $\boldsymbol{u}_O = (0, 1, 0, 0)^T$ and $\boldsymbol{u}_C = (1, 0, 1, 1)^T$, respectively.

Figure 16 shows representative solutions to the time-dependent advection-reaction equations (Eq. 54 in Appendix C) for the joint probability densities (ρ_{C_1}, ρ_O, ρ_{C_2}, and ρ_{C_3}) of the four-state model including both Ca^{2+} activation and Ca^{2+} inactivation (Eq. 51). The integration was performed for sufficiently long time that the profiles are approximate solutions to the generalized *time-independent* advection-reaction equations (see Eq. 57 in Appendix C). In Fig. 16A channel kinetics were chosen so that Ca^{2+}-activation was much faster process than inactivation ($k_a^\pm, k_c^\pm >> k_b^\pm, k_d^\pm$). Thus, states C_1 and O (similarly, C_3 and C_2) will equilibrate faster than the transitions $C_1 \leftrightharpoons C_3$ and $O \leftrightharpoons C_2$. When the domain time constant is very fast compared to channel kinetics (Fig. 16A, τ small, 0.1 s), the joint probability density functions for domain $[Ca^{2+}]$ accumulate near c_∞ when the channel is closed (C_1, C_2, C_3) and c_{ss} when the channel is open (O). Conversely, when the domain time constant is very slow compared to channel kinetics (Fig. 16A, τ large, 300 s), the joint probability density functions for domain $[Ca^{2+}]$ all appear Gaussian. This is similar to what was observed using both the Ca^{2+}-activated and Ca^{2+}-inactivated two-state models (Figs. 9 and

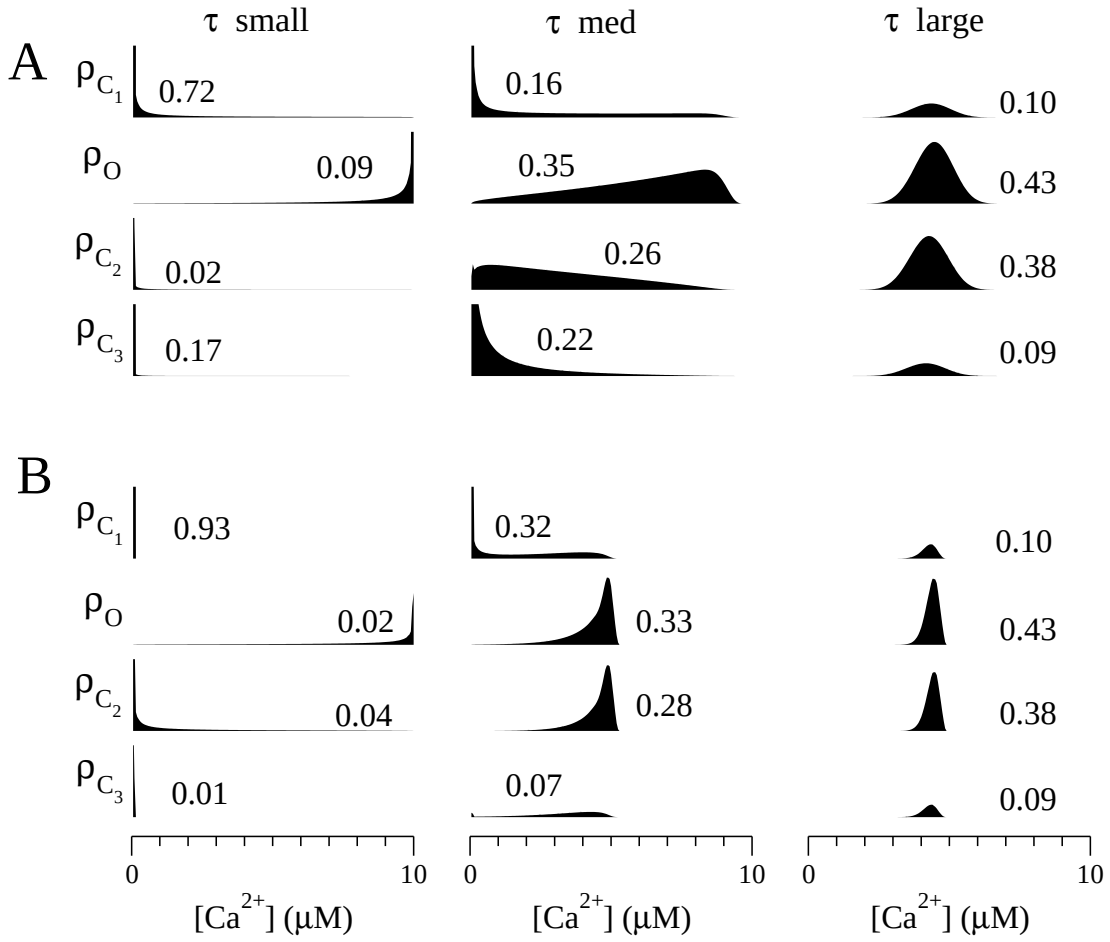

Figure 16: The joint probability densities $(\rho_{C_1}, \rho_O, \rho_{C_2}, \rho_{C_3})$ for the four-state model that includes both Ca^{2+}-activation and Ca^{2+}-inactivation (Eq. 51). The curves on each panel show results using a small (*dotted line*), intermediate (*solid line*) or large (*dashed line*) domain time constant (τ). A: Ca^{2+}-activation is much faster than Ca^{2+}-inactivation. Parameters: $\alpha_O = 9.95$ μM/s; $k_a^+ = 1$ $\mu M^{-1}s^{-1}$; $k_a^- = 1$ s^{-1}; $k_b^+ = 0.01$ $\mu M^{-1}s^{-1}$; $k_b^- = 0.05$ s^{-1}; $k_c^+ = k_a^+$; $k_c^- = k_a^-$; $k_d^+ = k_b^+$; $\tau =$ 0.1, 10, 300 s. B: Ca^{2+}-activation is much slower than Ca^{2+}-inactivation. Parameters: $\alpha_O = 9.95$ μM/s; $k_a^+ = 0.01$ $\mu M^{-1}s^{-1}$; $k_a^- = 0.01$ s^{-1}; $k_b^+ = 1$ $\mu M^{-1}s^{-1}$; $k_b^- = 5$ s^{-1}; $k_c^+ = k_a^+$; $k_c^- = k_a^-$; $k_d^+ = k_b^+$; $\tau = 0.03$, 100, 1000 s.

10). However, the curves of Fig. 16A have a more interesting form when the domain time constant is an intermediate value—slow compared to Ca^{2+} activation but fast compared to Ca^{2+} inactivation (τ medium, 10 s). Here the joint probability functions for domain $[Ca^{2+}]$ either diverge or can be quite broad depending on channel state. Of course, it remains the case that the domain $[Ca^{2+}]$ is likely to be greater when the channel is open.

Fig. 16B is similar to Fig. 16A except that here the Ca^{2+} activation process is *slower* than Ca^{2+} inactivation ($k_a^\pm, k_c^\pm << k_b^\pm, k_d^\pm$). These parameters are not chosen for physiologically

realism but to demonstrate that the association (k_i^+) and dissociation (k_i^-) rate constants in the four state model may influence the steady-state joint probability distributions (ρ_{C_1}, ρ_O, ρ_{C_2}, and ρ_{C_3}) even when the dissociation constants ($K_i = k_i^-/k_i^+$) remain unchanged (compare the τ medium case of Figs. 16A and B). Also note that the rapid equilibration between pairs of states does not necessarily imply that the joint probability distributions are of similar shape (compare ρ_{C_1} and ρ_O in the τ medium case of Fig. 16A).

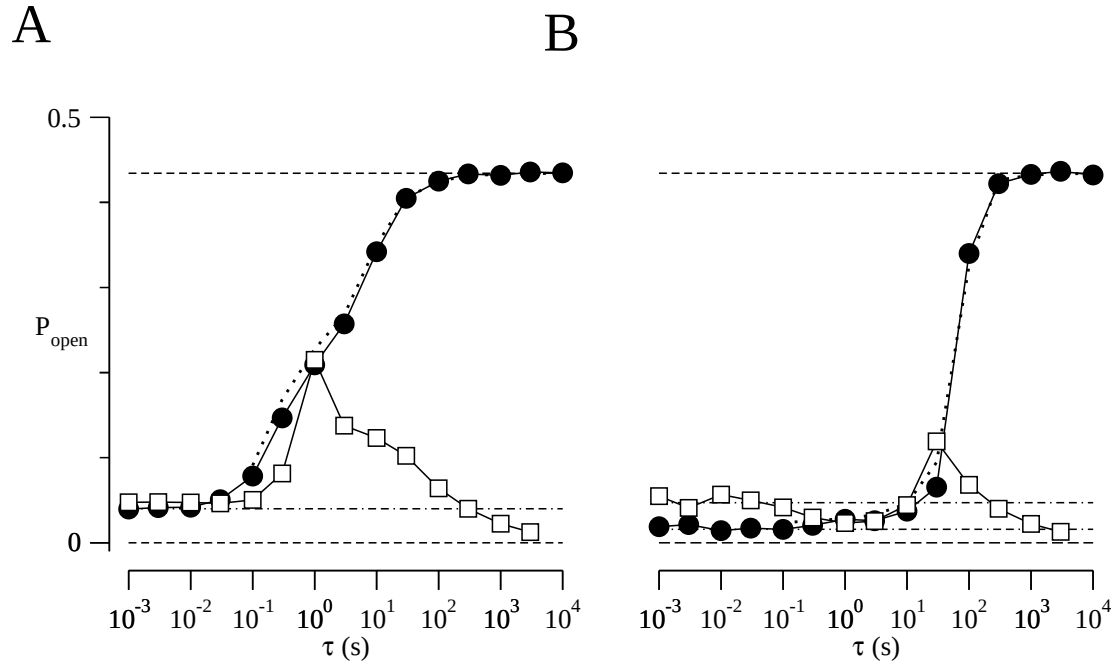

Figure 17: p_{open} as a function of τ using a four-state model with fast activation, slow inactivation (A) or fast inactivation and slow activation (B). The *filled circles* indicate results when the steady state [Ca^{2+}] (c_{ss}) is fixed, while the *open squares* show the case where the source amplitude (α_0) is held constant. The *dotted lines* show p_{open} of the generalized probability density calculation for the c_{ss} fixed case. The small and large τ limit of p_{open} for each case is also shown (*dot-dashed* and *dashed lines*). Parameters as Fig. 16.

Fig. 17A and B summarize the relationship between the equilibrium open probability (p_{open}) and domain time constant (τ) for the four-state model in both configurations presented above, that is, when Ca^{2+} activation is fast compared to inactivation (A) and the reverse case (B). The *filled circles* show the result of Monte Carlo simulation when the steady state [Ca^{2+}] (c_{ss}) is fixed, while the *open squares* repeat these calculations using fixed source amplitude (α_0). The *dot-dashed* and *dashed lines* provide analytical estimates in the small and large τ limits, respectively. The *dotted lines* show that the generalized probability den-

sity method (Fig. 16 and Appendix C) agrees with the Monte Carlo result (results are shown for $\tau \geq 0.03$ s where a 40 hr calculation resulted in a final integration time of 500 s or more). Consistent with our results for the DeYoung-Keizer model, when c_{ss} is constant p_{open} increases monotonically, in spite of the fact that the equilibrium probability of the four-state model is a bell-shaped function of the background [Ca^{2+}] (not shown). At intermediate values of the domain time constant (0.1 s $\leq \tau \leq$ 10 s), the observed open probability is greater when the four-state model includes fast activation and slow inactivation (Fig. 17A) as compared to the reverse case (Fig. 17B). In marked distinction from the results for the DeYoung-Keizer model, when we fix α_0 the four-state model exhibits an initial rise and eventual fall in p_{open} in the fast activation/slow inactivation case (*open squares* of Fig. 17), whereas when Ca^{2+} inactivation is fast and Ca^{2+} activation is slow p_{open} initially decreases, then increases, and finally decreases again to the limiting value of $p_{open} = 0$. Thus, when channel models include multiple time scales for channel kinetics, the effect of residual Ca^{2+} can be quite complex (Fig. 17) or comparatively simple (cf. Fig. 11).

Note that the dissociation constants (K_i) of the four-state model used in Fig. 17A and B are identical. Thus, the observed differences in p_{open} as a function of the domain time constant (e.g., the τ medium case) illustrate that the effect of residual Ca^{2+} on channel open probability can not be determined by the equilibrium properties of single channel models alone. In fact, when channel models include one or more cycles, even the limiting probabilities calculated using the method presented in Section 3.4 (the small and large τ limits) may depend on the association and dissociation rates constants and not just their ratios ($K_i = k_i^-/k_i^+$).

4 Discussion

While several groups have presented simulations of one or more Ca^{2+} channels stochastically gating under the influence of a time-dependent or time-independent Ca^{2+} domain (Sherman *et al.*, 1990; Mazzanti *et al.*, 1991; Bertram *et al.*, 1999; Rios & Stern, 1997; Swillens *et al.*, 1998; Swillens *et al.*, 1999; Stern *et al.*, 1999; Shuai & Jung, 2002; Shuai & Jung, 2003; Falcke, 2003*a*; Wang *et al.*, 2004), this study of the temporal effect of residual Ca^{2+} from previous channel openings on the stochastic gating of Ca^{2+}-regulated Ca^{2+} channels introduces several novel modeling approaches designed to investigate how that time scales of channel kinetics and Ca^{2+} domain formation and collapse influence channel open probability. In contrast with studies of the emergent phenomenon of synchronous gating of clustered Ca^{2+} channels (Swillens *et al.*, 1999; Nguyen *et al.*, 2004; Wang *et al.*, 2004), our aim here was to develop

a deeper understanding of the interaction between the gating of individual Ca^{2+}-regulated Ca^{2+} channels and a dynamic Ca^{2+} domain. Previous work focusing on the time scales associated with Ca^{2+} domains have often ignored stochastic effects of calcium release (Smith *et al.*, 1996; Thul & Falcke, 2004) or focused on whole-cell calcium dynamics (Wagner & Keizer, 1994; Falcke, 2003*b*).

One achievement of this study is the development of a general method for estimating the equilibrium open probability of single channel models coupled to a Ca^{2+} domain that is either very fast or slow compared to channel gating (Sections 3.2 and 3.4). We confirmed the validity of this method by Monte Carlo simulation of minimal two-state channel models either activated or inactivated by Ca^{2+} as well as the more realistic De Young-Keizer IP_3R model and a four-state model that includes both processes. This approach is applicable regardless of whether the domain is modeled using ordinary differential equations for the $[Ca^{2+}]$ in a restricted cytosolic compartment or using partial differential equations for the buffered diffusion of intracellular Ca^{2+} near the channel.

The probability density formulation for the effect of residual Ca^{2+} on the stochastic gating of Ca^{2+}-regulated Ca^{2+} channels was inspired by previously published mathematical models of synaptic transmitter release (Bertram & Sherman, 1998) and neuronal population dynamics (Nykamp & Tranchina, 2000). When this method was applied to minimal two-state Ca^{2+}-activated or Ca^{2+}-inactivated channels (Section 3.3), we obtained analytical expressions for p_{open} as a function channel parameters ($k^{\pm}$) and domain time constant (τ). This method can be generalized to more complicated channel models (Section 3.7 and Appendix C) and is an alternative to Monte Carlo simulation. The probability density approach is applicable when an ordinary differential equation describes the dynamics of domain $[Ca^{2+}]$ but, unfortunately, it is not straightforward to extend the method to situations where the Ca^{2+} domain is represented by reaction-diffusion equations.

— ◇ ◇ ◇ —

We found that the effect of residual Ca^{2+} on Ca^{2+}-regulated Ca^{2+} channels—even minimal two-state models—is not always intuitive. For example, when the source amplitude (α_0) is adjusted so that Ca^{2+} domain size (c_{ss}) is fixed, the two-state channel results indicate that Ca^{2+}-mediated $C \to O$ and $O \to C$ transitions considered in isolation both lead to p_{open} being an increasing function of τ. This suggested to us that the effect of residual Ca^{2+} on open probability of more complicated single channel models would be difficult to predict and motivated the development of the probability density formulation and estimates of p_{open} applicable to fast and slow domains. In the case of the De Young-Keizer IP_3R model,

we hypothesized that there would be a bell-shaped dependence of p_{open} on the domain time constant (τ), but found instead that p_{open} is a monotonically increasing or decreasing function of τ depending on whether the Ca^{2+} domain size (c_{ss}) or source amplitude (α_0) is fixed. More complex results are obtained for the four-state model that includes both Ca^{2+}-activation and Ca^{2+}-inactivation (Fig. 17). We found it counter-intuitive that the De Young-Keizer IP_3R model p_{open} vs. τ result is monotonic when α_0 is fixed. However, this result only underscores the fact that it is not possible to predict the effect of residual Ca^{2+} on the open probability of complicated single channel models without Monte Carlo simulation or the generalized probability density approach (Appendix C).

This study has deepened our intuition regarding the qualitative effect of residual Ca^{2+} on the relatively minimal single channel models. However, some consistently observed qualitative aspects of our results are *not* true in general. For example, for the four different channel models presented here the observed open probability of channels gating under the influence of a fast domain was always less than p_{open} with a slow domain when c_{ss} is fixed. Never-the-less, it is possible to construct single channel models for which this is not the case (see Appendix E).

Quantitative estimates of the effect of residual Ca^{2+} on channel open probability require Monte Carlo simulation or one of the novel methods presented here. Indeed, even qualitative aspects of the p_{open} vs. τ parameter studies are sometimes difficult to predict when the channel kinetics involve multiple time scales (recall the tri-phasic α_0 fixed case in Fig. 17B). Furthermore, a comparison of Fig. 16A and B (or Fig. 17A and B) demonstrates that the effect of residual Ca^{2+} can not be determined from equilibrium properties of single channel models alone—the only difference between panels A and B is whether Ca^{2+}-activation or Ca^{2+}-inactivation is the faster process. Still, the intuition gained from the minimal two-state models is often helpful for understanding the effect of residual Ca^{2+} on Ca^{2+}-regulated channels with more than two states (especially when c_{ss} is fixed).

— ◇ ◇ ◇ —

While plasma membrane ion channels in a small cell experience essentially the same time-course of membrane voltage, intracellular Ca^{2+} channels experience radically different local [Ca^{2+}], even during global Ca^{2+} responses. Importantly, the simulations presented here demonstrate that the traditional approach of using deterministic ordinary differential equations for the fraction of intracellular Ca^{2+} channels in each state may not always be appropriate, even when Ca^{2+}-regulated Ca^{2+} channels are diffusely distributed within cells and do not strongly interact with one another via buffered Ca^{2+} diffusion. Depending on

the channel model and dynamics of domain [Ca^{2+}], deterministic average rate equations will ignore the effect of residual Ca^{2+} from previous channel openings and incorrectly estimate the equilibrium open probability and, presumably, non-equilibrium dynamics as well.

An interesting avenue of future research is to explore whether the probability density approach presented here can be modified to represent a large number of intracellular Ca^{2+} channels diffusely distributed throughout a cell, each gating in response to it's own dynamic Ca^{2+} domain and also coupled to the another channels via changes in the bulk [Ca^{2+}]. Whole cell models that incorporate the probability density approach presented here might be able to realistically account for the distribution of local Ca^{2+} concentrations experienced by individual channels without the computational complexity of whole cell models based on Monte Carlo simulation of channel gating and/or three dimensional diffusion. This proposed modeling technique could be compared and contrasted to Langevin formulations of whole cell Ca^{2+} responses (Shuai & Jung, 2002; Shuai & Jung, 2003). Both approaches would assume a large number of intracellular Ca^{2+} channels and coupling, but the probability density approach suggested here would distinguish itself by providing a minimal representation of the different local Ca^{2+} concentrations experienced by the diffusely distributed intracellular channels.

In many cell types the opening of intracellular Ca^{2+} channels clustered at Ca^{2+} release sites is the basis of regenerative Ca^{2+} release. For this reason, it would be valuable to extend the probability density approach to situations where multiple channels are locally coupled. Most prior work analyzing the feedback of Ca^{2+} microdomains on clusters of intracellular Ca^{2+} channels has been based entirely on Monte Carlo simulation (Swillens *et al.*, 1998; Swillens *et al.*, 1999) or assumed "instantaneous coupling" (Nguyen *et al.*, 2004), the later approximation corresponding to the fast domain (small τ) limit discussed here. Interestingly, the probability density approach could be easily extended to analyze the dynamics of Ca^{2+} release from clusters of Ca^{2+} channels interacting with a time-dependent Ca^{2+} domain under the assumption of mean field coupling (Shuai & Jung, 2002; Shuai & Jung, 2003), a simplification that can be rigorously justified under some conditions (Nguyen *et al.*, 2004). The numerical and analytical work presented here is significant in part because it is an important first step toward understanding the effect of residual Ca^{2+} on clusters of Ca^{2+}-regulated Ca^{2+} channels. However, it does not appear to be straightforward to extend the probability density approach to clusters of Ca^{2+} regulated Ca^{2+} channels while at the same time preserving information about the spatial arrangement of the channels.

Our calculations suggest that the effect of exogenous Ca^{2+} buffers on the stochastic gating of Ca^{2+}-regulated Ca^{2+} channels is dependent in a complicated way on the details

of single channel kinetics and the subcellular geometry of the problem of interest. There is ample support for this experimentally. For example, in cardiac myocytes there is a high degree of variability in Ca^{2+} spark measures (such as brightness and frequency) that may be due to regulatory modulation of intracellular channels and different numbers or spatial arrangement of channels at Ca^{2+} release sites (Parker & Wier, 1997). This study would suggest two other possibilities: 1) variable size of the subsarcolemmal space (a restricted compartment that would influence the domain time constant) and 2) the effect of localized changes buffer concentration influencing the dynamics of residual Ca^{2+}. To give another example, in *Xenopus* oocytes a subpopulation of Ca^{2+} release sites that are particularly close to mitochondria exhibit lower Ca^{2+} puff activity than Ca^{2+} puff sites in regions of lower mitochondrial density (Marchant *et al.*, 2002). While the reason for this difference is unknown, one possibility is that the dynamics of residual Ca^{2+} interacting with Ca^{2+} release sites that are closely apposed to mitochondria is affected by the geometry of this association (i.e., the size of a restricted cytoplasmic space) or mitochondrial Ca^{2+} fluxes, both of which would influence the domain time constant experience by intracellular Ca^{2+} channels.

It is important to note that a Ca^{2+} domain is either "fast" or "slow" only in comparison to the rate constants of the Ca^{2+}-regulated Ca^{2+} channel in question. Thus, experimental and theoretical work indicating that domain Ca^{2+} concentration can increase or decrease by orders of magnitude in microseconds to milliseconds (Neher, 1986; Naraghi & Neher, 1997; Smith, 1996; Smith *et al.*, 1996; Thul & Falcke, 2004) should not be interpreted as evidence for the fast domain limit being more relevant that the slow domain limit. Rather, it is clear from dimensional analysis that the *relative size* of the domain time constant and various channel dwell times determines whether the fast or slow domain limit is relevant (recall the dimensionless parameters $\tau^{\pm} = \tau k^{\pm}$ in Eqs. 38–39 and Eqs. 41–42). In our parameter studies we focused on changing the domain time constant (τ) rather than the channel rate constants ($k_i^{\pm}$). This was not only done because parameter studies involving one parameter are easy to interpret, but also because the cytosolic milieu is potentially under experimental control (John *et al.*, 2001; Dargan & Parker, 2003). When exogenous Ca^{2+} buffers are absent, the time scale of Ca^{2+} domains may never-the-less be quite variable due to changing expression levels of endogenous Ca^{2+} binding proteins and the co-localization of Ca^{2+} channels with buffers that have distinct spatial distributions and binding kinetics (Dargan *et al.*, 2004).

— ◇ ◇ ◇ —

When the Ca^{2+} domain is modeled using the the cable equation, the parameter θ is inversely proportional to the free buffer concentration far from the channel (Eq. 13). When

the cytosol is in this excess buffer limit, experimental manipulations that increase the buffer concentration still further will decrease both θ and λ (assuming $D_c = \lambda^2/\theta$ is fixed). This will decrease the maximum domain $[Ca^{2+}]$ (c_{ss}) and also change the spatio-temporal dynamics of the domain. The simulations shown here indicate that the effect of such manipulations on single channel gating will depend on the specific details of channel kinetics. One test of the realism of single channel models is whether or not they can be used to predict or explain observed changes in p_{open} when the magnitude and dynamics of Ca^{2+} domains are experimentally perturbed. Even if changing single channel kinetics is below resolution of experiments, it's still important to understand the degree to which calcium buffering can influence the stochastic gating of Ca^{2+}-regulated Ca^{2+} channels (John *et al.*, 2001; Dargan & Parker, 2003).

Of course, the excess buffer approximation used here is an idealization of the buffered diffusion of intracellular Ca^{2+} as it actually occurs in cells. We focused on this limit in part because the reaction terms of the cable equation are identical to the right hand side of the ordinary differential equation representing the domain $[Ca^{2+}]$ in the restricted cytosolic domain case. An obvious extension of the Monte Carlo studies presented here is to include a realistic panel of Ca^{2+} buffers and the full equations for the buffered diffusion of intracellular Ca^{2+}—or, alternatively, the rapid buffer approximation (Wagner & Keizer, 1994; Smith *et al.*, 2001)—to describe the dynamics of the Ca^{2+} domain. While the probability density approach presented here can not be applied to spatially extended Ca^{2+} domains, it should be a simple matter to increase the realism of restricted compartment formulations by including multiple buffers.

Acknowledgments

This work was supported in part by National Science Foundation Molecular and Cell Biology CAREER award #0133132, NSF Integrative Biology and Neuroscience grant #0228273, and the Thomas F. and Kate Miller Jeffress Memorial Trust. Christopher J. Tignanelli was supported in part by the Undergraduate Science Education and Research Program at W&M funded by the Howard Hughes Medical Institute. The work as performed in part using computational facilities at the College of William and Mary enabled by grants from the NSF and Sun Microsystems. The fast Ca^{2+} domain results presented in Appendix D previously appeared in an invited book chapter (Smith, 2002*b*). Thanks to Jie Zhang for constructing Fig. 2.

Appendix A: An Exact Simulation Method

In addition to the Monte Carlo simulation methods for stochastically gating ion channels presented in Section 2.4, we have also employed exact simulation methods that have no intrinsic time-step (not shown). The method involves calculating the density of dwell times for a channel stochastically gating in the presence of a dynamic Ca^{2+} domain. Pseudo-random numbers consistent with this density are then generated to give the times of state changes.

We illustrate the exact simulation method with the two-state channel activated by Ca^{2+} (recall Eq. 1). Writing T_O as a random variable for the dwell time in the closed state, the constant $O \to C$ transition rate (k^-) implies that T_O is exponentially distributed with parameter (and mean) $1/k^-$. A pseudo-random number T_O can be calculated from $T_O = -\ln(X)/k^-$ where X is a uniform random number in the interval $0 \leq X \leq 1$ (Smith, 2002*a*).

While the the $O \to C$ transition rate is constant, the $C \to O$ transition rate is given by $k^+c(t)$ where $c(t) = c_\infty + (c_0 - c_\infty)\, e^{-t/\tau}$ and c_0 is the (often elevated) $[Ca^{2+}]$ at the time of the last $O \to C$ transition that we define as $t = 0$. Thus, the $C \to O$ transition rate, $\kappa(t)$, includes the effect of the dissipation of any residual Ca^{2+} and decays exponentially from an elevated value ($\kappa_0 = k^+c_0$) to the rate in the absence of a source for Ca^{2+} ($\kappa_\infty = k^+c_\infty$),

$$\kappa(t) = \kappa_\infty + (\kappa_0 - \kappa_\infty)\, e^{-t/\tau}.$$

This implies that the complement of the cumulative distribution function for T_C is given by,

$$\mathsf{P}\{T_C > t\} = \exp\left\{-\int_0^t \kappa(s)ds\right\} = \exp\left\{-\kappa_\infty t - \frac{1}{\tau}(\kappa_0 - \kappa_\infty)\left(1 - e^{-t/\tau}\right)\right\}. \qquad (53)$$

Because $\bar{F}(t) = \mathsf{P}\{T_C > t\}$ is a continuous function, Eq. 53 can be inverted and a pseudo-random number T_C can be produced using the inverse transformation method (Ross, 1988, pp. 389–390) in which T_C is given by $T_C = \bar{F}^{-1}(X)$ where X is uniformly distributed on the interval $0 \leq X \leq 1$.

Appendix B: Exact Solution Using Arbitrary Cooperativity

Equations 38 and 39 give the steady-state joint probability densities for the two-state Ca^{2+}-activated channel (Eq. 1) under the assumption that the cooperativity of Ca^{2+} binding is η

$= 1$. When the cooperativity, η is an integer greater than 1, the derivation is only slightly more complicated. Beginning with Eq. 35, we separate variables and integrate to obtain

$$\ln \rho_O - \ln \bar{\rho}_O = \left(1 - \tau^-\right) \int_{\bar{c}}^{c} \frac{d\hat{c}}{c_{ss} - \hat{c}} + \tau^+ \int_{\bar{c}}^{c} \frac{\hat{c}^\eta d\hat{c}}{\hat{c} - c_\infty}$$

where $\bar{c}$ is some point on the interior ($c_\infty < \bar{c} < c_{ss}$). As before, the first integral is

$$\left(\tau^- - 1\right) \ln \left(\frac{c_{ss} - c}{c_{ss} - \bar{c}} \right)$$

where we have eliminated absolute value signs in the logarithms using $c \leq c_{ss}$. Using the binomial coefficients and change of variables $v = \hat{c} - c_\infty$, the second integral becomes

$$\tau^+ \int_{\bar{c}-c_\infty}^{c-c_\infty} \sum_{i=0}^{\eta} \frac{\eta!}{(\eta - i)!i!} v^{\eta-i-1} c_\infty^i dv = \begin{cases} \tau^+ c_\infty^\eta \ln \left(\dfrac{c - c_\infty}{\bar{c} - c_\infty} \right) & \text{when} \quad i = \eta \\ h(c) & \text{when} \quad i \neq \eta \end{cases}$$

where

$$h(c) = \tau^+ c_\infty^\eta \ln \left(\frac{c - c_\infty}{\bar{c} - c_\infty} \right) + \tau^+ \sum_{i=0}^{\eta-1} \frac{\eta!}{(\eta - i)!i!} \cdot \frac{c_\infty^i}{\eta - i} \left[(c - c_\infty)^{\eta-i} - (\bar{c} - c_\infty)^{\eta-i} \right].$$

Exponentiating these expressions and using Eq. 34 gives ρ_C and ρ_O for integer $\eta \geq 2$,

$$\begin{aligned} \rho_C &= \hat{\rho} e^{h(c)} \left(c_{ss} - c\right)^{\tau^-} \left(c - c_\infty\right)^{\tau^+ c_\infty^\eta - 1} \\ \rho_O &= \hat{\rho} e^{h(c)} \left(c_{ss} - c\right)^{\tau^- - 1} \left(c - c_\infty\right)^{\tau^+ c_\infty^\eta}. \end{aligned}$$

For example, when the cooperativity of Ca^{2+} binding is $\eta = 2$, $h(c)$ is given by,

$$h(c) = \tau^+ \left[\frac{1}{2} \left(c - c_\infty\right)^2 + 2c_\infty \left(c - c_\infty\right) \right]$$

and the joint probability densities are

$$\begin{aligned} \rho_C &= \hat{\rho} \exp \left\{ \frac{1}{2} \tau^+ c \left(c + c_\infty\right) \right\} \left(c_{ss} - c\right)^{\tau^-} \left(c - c_\infty\right)^{\tau^+ c_\infty^2 - 1} \\ \rho_O &= \hat{\rho} \exp \left\{ \frac{1}{2} \tau^+ c \left(c + c_\infty\right) \right\} \left(c_{ss} - c\right)^{\tau^- - 1} \left(c - c_\infty\right)^{\tau^+ c_\infty^2} \end{aligned}$$

where the constant factors involving $\bar{c}$ and c_∞ have been absorbed into the constant $\hat{\rho}$ that must satisfy conservation of probability (Eq. 32).

Appendix C: Probability density approach for the effect of residual Ca^{2+} on arbitrarily complex channel models

Using an approach similar to Section 3.3, we can derive conservation equations for the joint probability densities to study the effect of residual Ca^{2+} on arbitrarily complex single channel models, assuming only that the generator matrix is of the form of Eq. 5.

Given a M-state single channel model of a Ca^{2+}-regulated Ca^{2+} channel of the form of Eq. 5 and $M \times 1$ column vectors $\boldsymbol{u}_C$ and $\boldsymbol{u}_O$ indicating closed and open states (see Section 2), we write $\rho_i(c)$ with $i = 1, 2, \cdots M$ for the joint probability density functions,

$$\rho_i(c,t)dc = \mathsf{P}\left\{c < [Ca^{2+}] < c + dc \text{ and } S(t) = \mathcal{S}_i\right\}.$$

Collecting the ρ_i into a $1 \times M$ row vector $\boldsymbol{\rho} = (\rho_1, \rho_2, \cdots, \rho_M)$, the system of advection-reaction equations satisfied by these probability densities can be written in matrix form as,

$$\frac{\partial \boldsymbol{\rho}}{\partial t} = -\frac{\partial}{\partial c}\left[\boldsymbol{\rho} J\right] + \boldsymbol{\rho} Q \tag{54}$$

where $\boldsymbol{\phi} = \boldsymbol{\rho} J$ is a $1 \times M$ row vector of probability fluxes and J is a $M \times M$ diagonal matrix formed from the scalar functions $j_C(c)$ and $j_O(c)$ given by Eqs. 24 and 25,

$$J(c) = \text{diag}\left\{j_C \boldsymbol{u}_C + j_O \boldsymbol{u}_O\right\}.$$

For example, for the two-state channel activated by Ca^{2+}, J is

$$J(c) = \begin{pmatrix} j_C & 0 \\ 0 & j_O \end{pmatrix} = \begin{pmatrix} -(c - c_\infty)/\tau & 0 \\ 0 & -(c - c_{ss})/\tau \end{pmatrix} = \frac{1}{\tau}\begin{pmatrix} c_\infty - c & 0 \\ 0 & c_{ss} - c \end{pmatrix}.$$

Conservation of probability for the densities ($\boldsymbol{\rho}$) solving Eq. 54 implies

$$\sum_{i=1}^{M} \pi_i = 1 \qquad \text{where} \qquad \pi_i = \int_{c_\infty}^{c_{ss}} \rho_i(c)dc \tag{55}$$

and because there may be more than one open state, the open probability of the channel is given by the inner product $p_{open} = \boldsymbol{\pi}\boldsymbol{u}_O$ where $\boldsymbol{\pi} = (\pi_1, \pi_2, \cdots, \pi_M)$.

The boundary conditions that we associate with Eq. 54 are again a consequence of enforcing zero probability flux at either c_∞ or c_{ss}, as appropriate for each element of $\boldsymbol{\phi} = \boldsymbol{\rho} J$. This leads to M boundary conditions for the vector of probability densities given by

$$\boldsymbol{\rho}_\infty \text{diag}\{\boldsymbol{u}_O\} + \boldsymbol{\rho}_{ss} \text{diag}\{\boldsymbol{u}_C\} = \boldsymbol{0}, \tag{56}$$

where $\boldsymbol{\rho}_\infty$ and $\boldsymbol{\rho}_{ss}$ are $\boldsymbol{\rho}(c)$ evaluated at $c = c_\infty$ and c_{ss}, respectively. For example, in the case of the two-state channel activated by Ca^{2+},

$$(\rho_C\ \rho_O)_\infty \begin{pmatrix} 0 & 0 \\ 0 & 1 \end{pmatrix} + (\rho_C\ \rho_O)_{ss} \begin{pmatrix} 1 & 0 \\ 0 & 0 \end{pmatrix} = (0\ 0)$$

in agreement with Eqs. 28 and 29.

Time-independent solutions of Eq. 54 satisfy the following linear system of first order differential equations,

$$0 = -\frac{d}{dc}\left[\boldsymbol{\rho} J\right] + \boldsymbol{\rho} Q.$$

Noting that $dJ/dc = -I/\tau$ and the general form for the generator matrix (Eq. 5), this can be written

$$\frac{d\boldsymbol{\rho}}{dc} = \boldsymbol{\rho}\left[\frac{1}{\tau} I + K_- + c^\eta K_+\right] J^{-1} = \boldsymbol{\rho} F \tag{57}$$

where the second equality defines $F(c)$. For the two-state Ca^{2+}-activated channel $F(c)$ is given by,

$$F(c) = \begin{pmatrix} \frac{1}{\tau} - k^+ c^\eta & k^+ c^\eta \\ k^- & \frac{1}{\tau} - k^- \end{pmatrix} \begin{pmatrix} \frac{\tau}{c_\infty - c} & 0 \\ 0 & \frac{\tau}{c_{ss} - c} \end{pmatrix} = \begin{pmatrix} \frac{1 - \tau^+ c^\eta}{c_\infty - c} & \frac{\tau^+ c^\eta}{c_{ss} - c} \\ \frac{\tau^-}{c_\infty - c} & \frac{1 - \tau^-}{c_{ss} - c} \end{pmatrix}$$

where once again we write $\tau^\pm = \tau k^\pm$. A little algebra shows that this is equivalent to Eqs. 30, 31, 35.

The steady-state probability densities describing the effect of residual Ca^{2+} on complex single channel models will solve the linear boundary value problem given by Eq. 57 with the associated boundary conditions (Eq. 56) and integral constraint (Eq. 55). Although the differential equation system is linear and homogeneous, $F(c)$ is not a constant coefficient matrix and is in fact singular at both endpoints (c_∞ and c_{ss}). For this reason Eq. 57 is not readily solved using numerical methods typically employed in the solution of boundary value problems. Instead, we implemented a finite difference scheme to numerically integrate the time-dependent system (Eq. 54), choosing an end-time sufficiently large to obtain the stationary densities satisfying $\partial\boldsymbol{\rho}/\partial t = 0$. Interestingly, we found that the second-order upwind scheme utilized in ensemble density calculations of integrate-and-fire neural networks (Nykamp & Tranchina, 2000) was inappropriate for this problem. However, a second order total variation diminishing scheme utilizing Roe's Superbee flux limiter worked well (Casti *et al.*, 2002; Hundsdorfer & Verwer, 2003). In particular, this numerical method could accommodate steep gradients and conserved probability even when the joint probability densities were delta-function-like and centered on the boundary values c_∞ and c_{ss} in the fast domain (small τ) limit.

Appendix D: Residual Ca^{2+} and separation of time scales in the De Young-Keizer IP_3R model

Li and Rinzel derived a simplified version of the De Young-Keizer model IP_3R by noticing that the fast processes of IP_3-potentiation and Ca^{2+}-activation are essentially at equilibrium with the slower process of Ca^{2+}-inactivation (Li & Rinzel, 1994). Without assuming the independence of IP_3R subunits, this fast/slow analysis can be applied to the 330 state De Young-Keizer IP_3R model presented in Section 2.2 leading to a five-state model (Smith, 2002*b*). Using this five-state model as a starting point, we can derive analytical estimates of the effect of residual Ca^{2+} on the De Young-Keizer IP_3R model that are approximations to the numerical estimate of Section 3.4 that utilized the 330×330 generator matrix.

The assumption that the fast processes of IP_3-potentiation and Ca^{2+}-activation are essentially at equilibrium with the slower process of Ca^{2+}-inactivation (Parker & Ivorra, 1990) leads to the following reduced transition-state diagram (Smith, 2002*b*),

$$\begin{array}{ccccccccc} & 4v_0^+ & & 3v_1^+ & & 2v_2^+ & & v_3^+ & \\ S_0 & \rightleftharpoons & S_1 & \rightleftharpoons & S_2 & \rightleftharpoons & S_3 & \rightleftharpoons & S_4 \\ & v_0^- & & 2v_1^- & & 3v_2^- & & 4v_3^- & \end{array} \tag{58}$$

where we have assumed $n = 4$ identical (but not independent) subunits. Note that this is the transition-state diagram for the entire channel. The lumped states S_i each corresponds to a channel with i inactivated subunits, that is, states S_1–S_4 are inactivated (and thus closed) while state S_0 is dis-inactivated (potentially open or closed). The v_i^+ and v_i^- in Eq. 58 are inactivation and dis-inactivation transition rates for a single subunit. In order to estimate p_{open} for the De Young-Keizer IP_3R in the presence of a fast or slow Ca^{2+} domain, we will assign values to the transition rates ($v_i^{\pm}$) so that their dependence on $[Ca^{2+}]$ and $[IP_3]$ is in agreement with Fig. 2, a Li-Rinzel-like quasi-static approximation, and our assumptions regarding the Ca^{2+} domain being fast or slow.

Consider first the case of a very fast Ca^{2+} domain (small τ). Here we follow Section 3.4 and associate a $[Ca^{2+}]$ (either c_∞ or c_{ss}) with each closed or open state. Because the inactivated De Young-Keizer IP_3R model (S_1–S_4) is necessarily closed, the appropriate concentration for these states is c_∞ and the transition rates for further Ca^{2+}-inactivation are

$$v_3^+ = v_2^+ = v_1^+ = (i_+ a_2 + i_- a_4)\, c_\infty = a_2 c_\infty,$$

where $i_+ = [IP_3]/([IP_3] + d_1)$ is the probability that a subunit is potentiated by IP_3 while not inactivated by Ca^{2+}, $i_- = 1 - i_+ = d_1/([IP_3] + d_1)$, and the second equality uses the rate

constant symmetry ($a_2 = a_4$) of the original De Young-Keizer model (De Young & Keizer, 1992). Similarly, the dis-inactivation transition probabilities do not depend on $[Ca^{2+}]$ and are given by,

$$v_3^- = v_2^- = v_1^- = v_0^- = h_+ b_2 + h_- b_4 = a_2 q_2,$$

where $h_+ = [IP_3]/([IP_3] + d_3)$, $h_- = 1 - h_+$, and $q_2 = d_2([IP_3] + d_1)/([IP_3] + d_3)$. On the other hand, the transition rates for Ca^{2+}-inactivation out of state S_0 is complicated by the possibility that the IP_3R is open and domain Ca^{2+} is elevated. Because v_0^+ is the transition rate for a single subunit and the channel can only be open if this subunit is in the permissive state (S_6), we can write

$$\begin{aligned} v_0^+ &= i_- a_4 c_\infty + i_+ c_- a_2 c_\infty + i_+ c_+ \left(1 - i_+^3 c_+^3\right) a_2 c_\infty + i_+^4 c_+^4 a_2 c_{ss} \\ &= a_2 \left\{ \left(1 - m_\infty^4\right) c_\infty + m_\infty^4 c_{ss} \right\} \end{aligned} \tag{59}$$

where $c_+ = c_\infty/(c_\infty + d_5)$ and $c_- = 1 - c_+$. Thus, we account for the possibility that the subunit inactivates under the influence of elevated domain Ca^{2+}, an event that will occur only if the IP_3R is open, that is, with probability

$$m_\infty^4 = i_+^4 \left(\frac{c_\infty}{c_\infty + d_5} \right)^4. \tag{60}$$

Notice that the expression for the inactivation rate of the fully dis-inactivated IP_3R (Eq. 59) is a weighted average of $4a_2c_\infty$ and $4a_2c_{ss}$ that depends on the conditional probability that the channel is open given that it is dis-inactivated (m_∞^4).

With the rate constants in Eq. 58 specified, p_{open} of this De Young-Keizer-like IP_3R model can be calculated. First, we find an expression for the equilibrium probability that the channel is dis-inactivated (i.e, in state S_0, which will be denoted by π_0). Because there are no cycles in Eq. 58, we apply the condition of detailed balance,

$$v_0^- \pi_1 = 4 v_0^+ \pi_0 \qquad 2 v_1^- \pi_2 = 3 v_1^+ \pi_1 \qquad 3 v_2^- \pi_3 = 2 v_2^+ \pi_2 \qquad 4 v_3^- \pi_4 = v_3^+ \pi_3$$

and solve for the stationary probabilities (π_i) with the conservation condition $\pi_0 + \pi_1 + \pi_2 + \pi_3 + \pi_4 = 1$. This leads to

$$\pi_0 = \frac{v_3 v_2 v_1 v_0}{v_3 v_2 v_1 v_0 + 4 v_3 v_2 v_1 + 6 v_2 v_1 + 4 v_1 + 1}$$

where $v_i = v_i^-/v_i^+$. Writing $v_\infty \equiv v_1 = v_2 = v_3 = q_2/c_\infty$ we have

$$\pi_0 = v_\infty^3 v_0 / D \qquad \text{where} \qquad D = v_\infty^3 v_0 + 4 v_\infty^3 + 6 v_\infty^2 + 4 v_\infty + 1,$$

and $q_2 = d_2\left([\mathrm{IP_3}] + d_1\right)/\left([\mathrm{IP_3}] + d_3\right)$. Similarly, $\pi_1 = 4v_\infty^3/D$, $\pi_2 = 6v_\infty^2/D$, $\pi_3 = 4v_\infty/D$, and $\pi_4 = 1/D$. The equilibrium open probability of the De Young-Keizer-like $\mathrm{IP_3R}$ model with domain $\mathrm{Ca^{2+}}$-mediated inactivation is thus given by $p_{open} = m_\infty^4\pi_0$ or

$$p_{open} = m_\infty^4\left(\frac{v_\infty^3 v_0}{v_\infty^3 v_0 + 4v_\infty^3 + 6v_\infty^2 + 4v_\infty + 1}\right) \tag{61}$$

where the effect of residual $\mathrm{Ca^{2+}}$ (in the case of a fast $\mathrm{Ca^{2+}}$ domain) occurs via the v_0 factor that is a function of both c_∞ and c_{ss} (Eq. 59).

It is now a simple matter to derive an analytical formula relevant to the case of a slow $\mathrm{Ca^{2+}}$ domain (large τ). In this case, the channel experiences the same $[\mathrm{Ca^{2+}}]$ regardless of state. Denoting this value by c^*, the conditional probability that the channel is open given that it is dis-inactivated is given by

$$m_*^4 = i_+^4\left(\frac{c_*}{c_* + d_5}\right)^4.$$

The open probability of the channel is found using an expression similar to Eq. 61, except that all $\mathrm{Ca^{2+}}$ concentrations are given by c_*, that is,

$$p_{open} = m_*^4\left(\frac{v_*^4}{v_*^4 + 4v_*^3 + 6v_*^2 + 4v_* + 1}\right) = m_*^4\left(\frac{v_*}{v_* + 1}\right)^4 \tag{62}$$

where $v_* = q_2/c_*$. In the large τ limit the open probability of the De Young-Keizer $\mathrm{IP_3R}$ receptor can be estimated by simultaneous solution of Eqs. 62 and 21.

These analytical approximations use separation of time scales between activation and inactivation in the De Young-Keizer model and are good approximations to the numerical estimates of Eqs. 45–48 that do not make this assumption. The *dot-dashed line* in Fig. 13A shows the least accurate of these results: when c_{ss} is fixed Eq. 60 and 61 slightly overestimate the p_{open} of the De Young-Keizer $\mathrm{IP_3R}$ model in the small τ limit. However, the three remaining limiting values indicated by the *solid* and *dotted lines* in Fig. 13 are visually indistinguishable from the estimates given by Eq. 60 and 61 (small τ) and Eqs. 62 and 21 (large τ).

Appendix E: p_{open} can be a decreasing function of τ

Using three different channel models that include $\mathrm{Ca^{2+}}$-activation, $\mathrm{Ca^{2+}}$-inactivation, or both, we find that p_{open} is an increasing function of domain time constant (τ) when the source amplitude of the channel (α_0) is varied so that domain size (c_{ss}) is fixed. However,

using the notation of Section 3.2, it is not necessarily the case that $\underline{p_{open}} < \overline{p_{open}}$, as can be seen by considering the following four-state model,

$$\begin{array}{ccccccc} & \overset{k_a^+ c}{} & & \overset{k_b^+ c}{} & & \overset{k_c^+ c}{} & \\ C_1 & \rightleftharpoons & O_1 & \rightleftharpoons & O_2 & \rightleftharpoons & C_2 \\ & \underset{k_a^-}{} & & \underset{k_b^-}{} & & \underset{k_c^-}{} & \end{array} \tag{63}$$

where the cooperativity of Ca^{2+} binding $\eta = 1$; $k_a^+ = 2$, $k_b^+ = 10$, $k_c^+ = 20$ $\mu M^{-1}s^{-1}$; and k_a^- $= 500$, $k_b^- = 50$ and $k_c^- = 200$ s^{-1}. In the case of a fast domain (small τ) the equilibrium open probability of this channel model is (Hill, 1977),

$$\underline{p_{open}} = \frac{k_a^+ c_\infty k_b^- k_c^- + k_a^+ c_\infty k_b^+ c_{ss} k_c^-}{k_a^- k_b^- k_c^- + k_a^+ c_\infty k_b^- k_c^- + k_a^+ c_\infty k_b^+ c_{ss} k_c^- + k_a^+ c_\infty k_b^+ c_{ss} k_c^+ c_{ss}}$$

which using the standard values of $c_\infty = 0.1$, $c_{ss} = 10$ μM gives $\underline{p_{open}} = 0.0012$. In the case of a slow domain (large τ) the equilibrium open probability is given by simultaneous solution of

$$p_{open} = \frac{k_a^+ c_* k_b^- k_c^- + k_a^+ c_* k_b^+ c_* k_c^-}{k_a^- k_b^- k_c^- + k_a^+ c_* k_b^- k_c^- + k_a^+ c_* k_b^+ c_* k_c^- + k_a^+ c_* k_b^+ c_* k_c^+ c_*}$$

and Eq. 21 giving $\overline{p_{open}} = 0.0004$ and $c_* = 0.1042$ μM. Thus, for this particular four-state model we find that $\underline{p_{open}} > \overline{p_{open}}$ even though c_{ss} is fixed.

In spite of this example, upon experimenting with many different channel models one does get the impression that $\underline{p_{open}} < \overline{p_{open}}$ is the usual result. This may be because in channel models without cycles and a single Ca^{2+}-mediated $C \to O$ transition, p_{open} must increase with τ when c_{ss} is fixed. In such cases, the small τ limit always leads to an expression of the form,

$$\underline{p_{open}} = \frac{\kappa_1 c_\infty^\eta}{\kappa_2 + \kappa_3 c_\infty^\eta},$$

while in the large tau limit we obtain,

$$\overline{p_{open}} = \frac{\kappa_1 c_*^\eta}{\kappa_2 + \kappa_3 c_*^\eta} \qquad \text{where} \qquad c_* = c_{ss}\overline{p_{open}} + c_\infty \left(1 - \overline{p_{open}}\right).$$

Because $c_\infty < c_* < c_{ss}$ we see that under the above assumptions $\underline{p_{open}} < \overline{p_{open}}$. Similar arguments can be made for models without cycles that contain multiple Ca^{2+}-mediated transitions when they are either all activating ($C \to O$) or all inactivating ($O \to C$). However, $\underline{p_{open}}$ can be greater than $\overline{p_{open}}$ when both activating and inactivating transitions are present (Eq. 63).

Table

Parameter	Value	Units	Parameter	Value	Units
a_1	400	$\mu\mathrm{M}^{-1}\mathrm{s}^{-1}$	d_1	0.13	μM
a_2	0.2	$\mu\mathrm{M}^{-1}\mathrm{s}^{-1}$	d_2	1.049	μM
a_3	400	$\mu\mathrm{M}^{-1}\mathrm{s}^{-1}$	d_3	0.9434	μM
a_4	0.2	$\mu\mathrm{M}^{-1}\mathrm{s}^{-1}$	d_4	d_1d_2/d_3	μM
a_5	20	$\mu\mathrm{M}^{-1}\mathrm{s}^{-1}$	d_5	0.08234	μM

Table 1: Parameters of the De Young-Keizer IP_3R model (De Young & Keizer, 1992). Dissociation rate constants b_i are given by $b_i = a_i d_i$.

References

Atri, A., Amundson, J., Clapham, D. & Sneyd, J. (1993). A single-pool model for intracellular Ca^{2+} oscillations and waves in the Xenopus laevis oocyte. *Biophys J,* **65** (4), 1727–39.

Bers, D. (1992). *Excitation-Contraction Coupling and Cardiac Contractile Force.* Second edition, Kluwer Academic Publishers.

Bertram, R. & Sherman, A. (1998). Population dynamics of synaptic release sites. *SIAM J Appl Math,* **58** (1), 142–169.

Bertram, R., Smith, G. & Sherman, A. (1999). Modeling study of the effects of overlapping Ca^{2+} microdomains on neurotransmitter release. *Biophys J,* **76** (2), 735–50.

Bezprozvanny, I. & Ehrlich, B. (1994). Inositol (1,4,5)-trisphosphate (IP_3)-gated Ca^{2+} channels from cerebellum: conduction properties for divalent cations and regulation by intraluminal Ca^{2+}. *J Gen Physiol,* **104** (5), 821–56.

Bezprozvanny, I., Watras, J. & Ehrlich, B. (1991). Bell-shaped Ca^{2+}-response curves of Ins(1,4,5)P3- and Ca^{2+}-gated channels from endoplasmic reticulum of cerebellum. *Nature,* **351** (6329), 751–4.

Cannell, M., Cheng, H. & Lederer, W. (1995). The control of calcium release in heart muscle. *Science,* **268** (5213), 1045–1049.

Casti, A., Omurtag, A., Sornborger, A., Kaplan, E., Knight, B., Victor, J. & Sirovich, L. (2002). A population study of integrate-and-fire-or-burst neurons. *Neural Comput,* **14** (5), 957–986.

Cheng, H., Lederer, W. & Cannell, M. (1993). Ca^{2+} sparks: elementary events underlying excitation-contraction coupling in heart muscle. *Science,* **262** (5134), 740–4.

Colquhoun, D. & Hawkes, A. (1995). A Q-matrix cookbook: how to write only one program to calculate the sigle-channel and macroscopic predictions for any kinetic mechanism. In *Single-Channel Recording*, (Sakmann, B. & Neher, E., eds), pp. 589–633. Plenum Press New York.

Dargan, S. & Parker, I. (2003). Buffer kinetics shape the spatiotemporal patterns of IP_3-evoked Ca^{2+} signals. *J Physiol,* **553** (Pt 3), 775–788.

Dargan, S., Schwaller, B. & Parker, I. (2004). Spatiotemporal patterning of IP_3-mediated Ca^{2+} signals in Xenopus oocytes by Ca^{2+}-binding proteins. *J Physiol,* **556** (Pt 2), 447–461.

De Young, G. & Keizer, J. (1992). A single-pool inositol 1,4,5-trisphosphate-receptor-based model for agonist-stimulated oscillations in Ca^{2+} concentration. *Proc Natl Acad Sci USA,* **89** (20), 9895–9.

Falcke, M. (2003*a*). On the role of stochastic channel behavior in intracellular Ca^{2+} dynamics. *Biophys J,* **84** (1), 42–56.

Falcke, M. (2003*b*). Buffers and oscillations in intracellular Ca^{2+} dynamics. *Biophys J,* **84** (1), 28–41.

Fierro, L. & Parekh, A. (1999). Fast Ca^{2+}-dependent inactivation of Ca^{2+} release-activated calcium current (CRAC) in RBL-1 cells. *J Membr Biol,* **168** (1), 9–17.

Fox, R. & Lu, Y. (1994). Emergent collective behavior in large numbers of globally coupled independently stochastic ion channels. *Physical Rev. E,* **49** (4), 3421–3431.

Fraiman, D. & Dawson, S. (2004). A model of IP_3 receptor with a luminal Ca^{2+} binding site: stochastic simulations and analysis. *Cell Calcium,* **35** (5), 403–413.

Hill, T. (1977). *Free Energy Transduction in Biology: The Steady-State Kinetic and Thermodynamic Formalism.* Academic Press, New York.

Hundsdorfer, W. & Verwer, J. (2003). *Numerical Solution of Time-Dependent Advection-Diffusion-Reaction Equations.* Springer-Verlag, Berlin.

John, L., Mosquera-Caro, M., Camacho, P. & Lechleiter, J. (2001). Control of IP_3-mediated Ca^{2+} puffs in xenopus laevis oocytes by the Ca^{2+}-binding protein parvalbumin. *J Physiol,* **535** (Pt 1), 3–16.

Joseph, S., Rice, H. & Williamson, J. (1989). The effect of external Ca^{2+} and pH on inositol trisphosphate-mediated Ca^{2+} release from cerebellum microsomal fractions. *Biochem J,* **258** (1), 261–5.

Kaftan, E., Ehrlich, B. & Watras, J. (1997). Inositol 1,4,5-trisphosphate (IP_3) and Ca^{2+} interact to increase the dynamic range of IP_3 receptor-dependent Ca^{2+} signaling. *J Gen Physiol,* **110** (5), 529–38.

Keizer, J. & Levine, L. (1996). Ryanodine receptor adaptation and Ca^{2+}-induced Ca^{2+} release-dependent Ca^{2+} oscillations. *Biophys J,* **71** (6), 3477–87.

LeBeau, A., Yule, D., Groblewski, G. & Sneyd, J. (1999). Agonist-dependent phosphorylation of the inositol 1,4,5-trisphosphate receptor: a possible mechanism for agonist-specific calcium oscillations in pancreatic acinar cells. *J Gen Physiol,* **113** (6), 851–72.

Li, Y., Keizer, J., Stojilkovic, S. & Rinzel, J. (1995). Ca^{2+} excitability of the ER membrane: an explanation for IP_3-induced Ca^{2+} oscillations. *Am J Physiol,* **269** (5 Pt 1), C1079–92.

Li, Y. & Rinzel, J. (1994). Equations for IP_3R-mediated $[Ca^{2+}]_i$ oscillations derived from a detailed kinetic model: a Hodgkin-Huxley like formalism. *J Theor Biol,* **166** (4), 461–73.

Mak, D. & Foskett, J. (1997). Single-channel kinetics, inactivation, and spatial distribution of inositol trisphosphate (IP_3) receptors in Xenopus oocyte nucleus. *J Gen Physiol,* **109** (5), 571–87.

Mak, D., McBride, S. & Foskett, J. (1998). Inositol 1,4,5-trisphosphate activation of inositol trisphosphate receptor Ca^{2+} channel by ligand tuning of Ca^{2+} inhibition. *Proc Natl Acad Sci USA,* **95** (26), 15821–5.

Marchant, J., Ramos, V. & Parker, I. (2002). Structural and functional relationships between Ca^{2+} puffs and mitochondria in Xenopus oocytes. *Am J Physiol Cell Physiol,* **282** (6), C1374–C1386.

Matveev, V., Zucker, R. & Sherman, A. (2004). Facilitation through buffer saturation: constraints on endogenous buffering properties. *Biophys J,* **86** (5), 2691–2709.

Mazzag, B., Nguyen, V. & Smith, G. (2004). Analysis of the effect of residual Ca^{2+} on the gating of Ca^{2+}-regulated Ca^{2+} channels. In *Biophysical Society Annual Meeting Abstracts, Program No. 579*, Baltimore, MD.

Mazzanti, M., DeFelice, L. & Liu, Y. (1991). Gating of L-type Ca^{2+} channels in embryonic chick ventricle cells: dependence on voltage, current and channel density. *J Physiol,* **443**, 307–334.

Moraru, I., Kaftan, E., Ehrlich, B. & Watras, J. (1999). Regulation of type 1 inositol 1,4,5-trisphosphate-gated calcium channels by InsP3 and Ca^{2+}: Simulation of single channel

kinetics based on ligand binding and electrophysiological analysis. *J Gen Physiol,* **113** (6), 837–849.

Naraghi, M. & Neher, E. (1997). Linearized buffered Ca^{2+} diffusion in microdomains and its implications for calculation of $[Ca^{2+}]$ at the mouth of a Ca^{2+} channel. *J Neurosci,* **17** (18), 6961.

Neher, E. (1986). Concentration profiles of intracellular Ca^{2+} in the presence of diffusible chelator. *Exp Brain Res,* **14**, 80–96.

Neher, E. (1998). Usefulness and limitations of linear approximations to the understanding of Ca^{2+} signals. *Cell Calcium,* **24**, 345.

Nguyen, V., Mathias, R. & Smith, G. (2004). A stochastic automata network descriptor for markov chain models of instantaneously-coupled intracellular Ca^{2+} channels. *Bull. Math. Biol.* . Submitted.

Norris, J. (1997). *Markov chains*. Cambridge University Press, Cambridge.

Nykamp, D. & Tranchina, D. (2000). A population density approach that facilitates large-scale modeling of neural networks: analysis and an application to orientation tuning. *J Comput Neurosci,* **8** (1), 19–50.

Parekh, A. (2003). Store-operated Ca^{2+} entry: dynamic interplay between endoplasmic reticulum, mitochondria and plasma membrane. *J Physiol,* **547** (Pt 2), 333–348.

Parker, I. & Ivorra, I. (1990). Inhibition by Ca^{2+} of inositol trisphosphate-mediated Ca^{2+} liberation: a possible mechanism for oscillatory release of Ca^{2+}. *Proc Natl Acad Sci USA,* **87** (1), 260–4.

Parker, I. & Wier, W. (1997). Variability in frequency and characteristics of Ca^{2+} sparks at different release sites in rat ventricular myocytes. *J Physiol,* **505** (Pt 2), 337–44.

Rios, E. & Stern, M. (1997). Ca^{2+} in close quarters: microdomain feedback in excitation-contraction coupling and other cell biological phenomena. *Annu Rev Biophys Biomol Struct,* **26**, 47–82.

Roberts, W. (1993). Spatial Ca^{2+} buffering in saccular hair cells. *Nature,* **363** (6424), 74–6.

Roberts, W. (1994). Localization of Ca^{2+} signals by a mobile Ca^{2+} buffer in frog saccular hair cells. *Nature,* **14** (5 Pt 2), 3246–62.

Ross, S. (1988). *A first course in probability.* Macmillan Publishing Company, New York.

Sherman, A., Keizer, J. & Rinzel, J. (1990). Domain model for Ca^{2+}-inactivation of Ca^{2+} channels at low channel density. *Biophys J,* **58** (4), 985–95.

Shuai, J. & Jung, P. (2002). Stochastic properties of Ca^{2+} release of inositol 1,4,5-trisphosphate receptor clusters. *Biophys J,* **83** (1), 87–97.

Shuai, J. & Jung, P. (2003). Optimal ion channel clustering for intracellular calcium signaling. *Proc Natl Acad Sci U S A,* **100** (2), 506–510.

Smith, G. (1996). Analytical steady-state solution to the rapid buffering approximation near an open Ca^{2+} channel. *Biophys J,* **71** (6), 3064–3072.

Smith, G. (2000). Modeling local and global Ca^{2+} signals using reaction-diffusion equations. In *Computational Neuroscience: Realistic Modeling for Experimentalists*, (DeSchutter, E., ed.), pp. 49–85. CRC Press.

Smith, G. (2002*a*). Modeling the stochastic gating of ion channels. In *Computational Cell Biology*, (Fall, C., Marland, E., Wagner, J. & Tyson, J., eds), pp. 291–325. Springer-Verlag.

Smith, G. (2002*b*). An extended DeYoung-Keizer-like IP_3 receptor model that accounts for domain Ca^{2+}-mediated inactivation. In *Recent Research Developments in Biophysical Chemistry, Vol. II*, (Condat, C. & Baruzzi, A., eds), pp. 37–55, Research Signpost.

Smith, G., Dai, L., Muira, R. & Sherman, A. (2001). Asymptotic analysis of equations for the buffered diffusion of intracellular Ca^{2+}. *SIAM J Appl Math,* **61** (5), 1816–1838.

Smith, G. & Keizer, J. (1998). Spark-to-wave transition: saltatory transmission of Ca^{2+} waves in cardiac myocytes. *Biophys Chem,* **72** (1-2), 87–100.

Smith, G., Keizer, J., Stern, M., Lederer, W. & Cheng, H. (1998). A simple numerical model of Ca^{2+} spark formation and detection in cardiac myocytes. *Biophys J,* **75** (7), 15–32.

Smith, G., Wagner, J. & Keizer, J. (1996). Validity of the rapid buffering approximation near a point source of Ca^{2+} ions. *Biophys J,* **70** (6), 2527–2539.

Sneyd, J. & Dufour, J. (2002). A dynamic model of the type-2 inositol trisphosphate receptor. *Proc Natl Acad Sci U S A,* **99** (4), 2398–2403.

Steeb, W.-H. (1997). *Matrix calculus and Kronecker product with applications and C++ programs.* World Scientific.

Stern, M., Song, L., Cheng, H., Sham, J., Yang, H., Boheler, K. & Rios, E. (1999). Local control models of cardiac excitation-contraction coupling. a possible role for allosteric interactions between ryanodine receptors. *J Gen Physiol,* **113** (3), 469–489.

Swillens, S., Champeil, P., Combettes, L. & Dupont, G. (1998). Stochastic simulation of a single inositol 1,4,5-trisphosphate-sensitive Ca^{2+} channel reveals repetitive openings during 'blip-like' Ca^{2+} transients. *Cell Calcium,* **23** (5), 291–302.

Swillens, S., Dupont, G., Combettes, L. & Champeil, P. (1999). From Ca^{2+} blips to Ca^{2+} puffs: theoretical analysis of the requirements for interchannel communication. *Proc Natl Acad Sci U S A,* **96** (24), 13750–13755.

Tang, Y., Stephenson, J. & Othmer, H. (1995). Simplification and analysis of models of Ca^{2+} dynamics based on IP_3-sensitive Ca^{2+} channel kinetics. *Biophys J,* **70** (1), 246–263.

Thul, R. & Falcke, M. (2004). Release currents of IP_3 receptor channel clusters and concentration profiles. *Biophys J,* **86** (5), 2660–2673.

Wagner, J. & Keizer, J. (1994). Effects of rapid buffers on Ca^{2+} diffusion and Ca^{2+} oscillations. *Biophys J,* **67**, 447–456.

Wang, K., Rappel, W. & Levine, H. (2004). Cooperativity can reduce stochasticity in intracellular calcium dynamics. *Phys Bio,* **1**, 27–34.

Zucker, R. & Regehr, W. (2002). Short-term synaptic plasticity. *Annu Rev Physiol,* **64**, 355–405.

Zweifach, A. & Lewis, R. (1995). Rapid inactivation of depletion-activated calcium current (ICRAC) due to local calcium feedback. *J Gen Physiol,* **105** (2), 209–226.